

Shell model study of the isobaric chains

$A = 50$, $A = 51$ and $A = 52$

A. Poves and J. Sánchez-Solano

*Departamento de Física Teórica C-XI, Universidad Autónoma de Madrid,
E-28049 Madrid, Spain*

E. Caurier and F. Nowacki

*Groupe de Physique Théorique, Centre de Recherches Nucléaires, Institut National
de Physique Nucléaire et de Physique des Particules, Centre National de la
Recherche Scientifique, Université Louis Pasteur, Boîte Postale 28, F-67037
Strasbourg Cedex 2, France*

Abstract

Shell model calculations in the full pf -shell are carried out for the $A=50$, 51 and 52 isobars. The most frequently used effective interactions for the pf -shell, KB3 and FPD6 are revisited and their behaviour at the $N=28$ and $Z=28$ closures examined. Cures to their -relatively minor- defaults are proposed, and a new mass dependent version called KB3G is released. Energy spectra, electromagnetic transitions and moments as well as beta decay properties are computed and compared with the experiment and with the results of the earlier interactions. A high quality description is achieved. Other miscellaneous topics are addressed; the Coulomb energy differences of the yrast states of the mirror pair ^{51}Mn - ^{51}Fe and the systematics of the magnetic moments of the $N=28$ isotones.

Key words: $A=50$, $A=51$, $A=52$, Shell Model, Effective interactions, Full pf -shell spectroscopy, Level schemes and transition probabilities, Gamow-Teller beta decays, Half-lives, Magnetic moments, Coulomb energy differences.

PACS: 21.10.-k, 27.40.+z, 21.60.Cs, 23.40.-s

1 Introduction

The pf -shell has been the focus of a lot of activity in nuclear structure during the last years. Prompted in some cases by the large scale shell model results, that indicated the presence of a region of deformation around ^{48}Cr [1–3], a lot of new experiments and calculations have been carried out, addressing many

different issues; deformed bands and band termination [4], yrast traps [5], high K isomers [6], coexistence of deformed bands of natural and non-natural parity [7], effects of neutron proton pairing [8], etc. A very recent highlight has been the discovery of an excited deformed band in ^{56}Ni [9] coexisting with the spherical states based in the doubly magic ground state. In addition to the exact shell model diagonalizations, the new Monte Carlo techniques, SMMC and MCSM have been extensively applied to this region [10–13]. Mean field descriptions of various kinds have also been used to explore different issues concerning this deformation region [14,15].

In this article we extend the full pf -shell calculations up to $A=52$. Detailed results for ^{50}Cr , ^{50}Mn and ^{52}Fe using KB3 have been already published in refs [5,16,17] and we will not deal with them here because the new interaction KB3G gives equivalent results. In the cases of ^{51}Cr , ^{52}Cr , ^{51}Mn and ^{52}Mn we have carried out the full pf -shell calculation for the yrast states only. To perform detailed spectroscopy in the full space would have demanded a huge amount of computer time, not justified by the improvement on the results, as we have checked. Hence, for the non-yrast states we shall present results in a truncated ($t=5$) space (no more than 5 particles are allowed to excite from the $1f_{7/2}$ subshell). At this truncation level, the most relevant states are sufficiently converged.

As we have discussed in detail elsewhere [3] our usual effective interaction KB3 [18,19] produces a quasiparticle gap in ^{56}Ni about 1 MeV too large. Approaching the doubly magic closure, the effects of this default become more visible. That is the reason why, in a recent study of the deformed excited band of ^{56}Ni [9], we used a preliminary modified version of KB3 in order to have the correct gap. This modified version of KB3 was also used in the study of the M1 strength functions of the $N=28$ isotones in ref. [20]. We shall examine the interaction issues in section II. In sections III, IV and V we present the spectroscopic results for $A=50$, 51 and 52 respectively. In section VI we gather the beta decay results. In section VII we discuss the Coulomb Energy Differences (CED) between the yrast states of the mirror pair $A=51$. Finally, in section VIII we study the behaviour of the magnetic moments of the $N=28$ isotones. We close with the conclusions.

Throughout the paper f stands for $f_{7/2}$ (except, of course, when we speak of the pf shell) and r , generically, for any or all of the other subshells ($p_{1/2}$ $p_{3/2}$ $f_{5/2}$). Spaces of the type

$$f^{n-n_0}r^{n_0} + f^{n-n_0-1}r^{n_0+1} + \dots + f^{n-n_0-t}r^{n_0+t} \quad (1)$$

represent possible truncations: n_0 is different from zero if more than 8 neutrons (or protons) are present and when $t = n - n_0$ we have the full space $(pf)^n$ for $A = 40 + n$.

The interaction KB3 is a (mostly) monopole modification of the original Kuo-Brown one [18]. The modifications are described in detail in [3].

In what follows, and unless specified otherwise, we use

- harmonic oscillator wave functions with $b = 1.01A^{1/6}$ fm;
- bare electromagnetic factors in $M1$ transitions; effective charges of $1.5 e$ for protons and $0.5 e$ for neutrons in the electric quadrupole transitions and moments;
- Gamow-Teller (GT) strength defined through

$$B(GT) = \left(\frac{g_A}{g_V}\right)_{\text{eff}}^2 \langle \sigma \tau \rangle^2, \quad \langle \sigma \tau \rangle = \frac{\langle f || \sum_k \sigma^k t_{\pm}^k || i \rangle}{\sqrt{2J_i + 1}}, \quad (2)$$

where the matrix element is reduced with respect to the spin operator only (Racah convention [21]), \pm refers to β^\pm decay, $t_{\pm} = (\tau_x \pm i\tau_y)/2$, with $t_+p = n$ and $(g_A/g_V)_{\text{eff}}$ is the effective axial to vector ratio for GT decays,

$$\left(\frac{g_A}{g_V}\right)_{\text{eff}} = 0.77 \left(\frac{g_A}{g_V}\right)_{\text{bare}}, \quad (3)$$

with $(g_A/g_V)_{\text{bare}} = 1.2599(25)$ [22];

- for Fermi decays we have

$$B(F) = \langle \tau \rangle^2, \quad \langle \tau \rangle = \frac{\langle f || \sum_k t_{\pm}^k || i \rangle}{\sqrt{2J_i + 1}}, \quad (4)$$

- half-lives, $T_{1/2}$, are found through

$$(f_A + f^\epsilon) T_{1/2} = \frac{6146 \pm 6}{(f_V/f_A)B(F) + B(GT)}. \quad (5)$$

We follow ref. [23] in the calculation of the f_A and f_V integrals and ref. [24] for f^ϵ . The experimental energies are used.

- The intrinsic quadrupole moments Q_0 are extracted from the spectroscopic ones through

$$Q_0 = \frac{(J+1)(2J+3)}{3K^2 - J(J+1)} Q_{\text{spec}}(J), \quad \text{for } K \neq 1 \quad (6)$$

or from the BE2's through the rotational model prescription

$$B(E2, J \rightarrow J-2) = \frac{5}{16\pi} e^2 |\langle JK20 | J-2, K \rangle|^2 Q_0^2, \quad \text{for } K \neq \frac{1}{2}, 1. \quad (7)$$

The diagonalizations are performed in the m -scheme using a fast implementation of the Lanczos algorithm through the code ANTOINE [25] or in J-coupled scheme using the code NATHAN [26]. Some details may be found in ref. [27].

The strength functions are obtained using Whitehead's prescription [28], explained and illustrated in refs. [29–31].

All the experimental results for which no explicit credit is given come from the electronic version of Nuclear Data Sheets compiled by Burrows [32].

2 The Interactions

Following ref. [33], we shall treat the effective interaction as a sum of a monopole and a multipole part. The monopole part is responsible for the energies of the closed shells (CS) and the closed shells plus or minus one particle (CS \pm 1). In our valence space, the starting point (or vacuum) is the ^{40}Ca core, and the single particle energies are provided by the levels of ^{41}Ca . The harmonic oscillator closure should be ^{80}Zr and its corresponding hole states in ^{79}Y . Nevertheless, and taking care of the effect of correlations, ^{48}Ca and ^{56}Ni can be also taken as reference closed shells. In this we are lucky, because the information given by ^{80}Zr is rather useless. For N,Z>32 the influence of the $1g_{9/2}$ orbit is very strong and the pf valence space is no longer valid. Around ^{80}Zr , the occupation of the orbits $1g_{9/2}$ and $2d_{5/2}$ drives the nuclei into deformed shapes [34,35]. There are no experimental results available for the single hole states in ^{79}Y . Even if some excited levels were accessible, a particle plus rotor spectrum should be expected, coming from the coupling of the holes to the ^{80}Zr deformed core. With this information missing, we have to rely on indirect indications, as those coming from spherical Hartree Fock calculations (not very accurate) or from the new monopole formulae fitted to the real shell closures and their particle and hole partners [36]. Hence, our main guidance to adjust the monopole part of our interactions comes from the gaps around ^{48}Ca and ^{56}Ni and from the single particle states of ^{49}Ca and ^{57}Ni . The multipole part of the interactions will be also analysed in terms of “coherent” multipoles, as proposed in ref. [33]. This part of the interaction is left unchanged.

The quasiparticle gap for ^{48}Ca is defined as

$$\Delta = 2BE(^{48}\text{Ca}) - BE(^{49}\text{Ca}) - BE(^{47}\text{Ca}) \quad (8)$$

and similarly for ^{56}Ni .

In table 1 we compare these quantities for the most popular effective interactions used in the pf -shell; KB3 [18,19] and FPD6 [37]. Both interactions use very similar single particle energies; $\epsilon_{7/2}=0.0$ MeV, $\epsilon_{3/2}=2.0$ MeV, $\epsilon_{1/2}=4.0$ MeV and $\epsilon_{5/2}=6.5$ MeV for KB3 and $\epsilon_{7/2}=0.0$ MeV, $\epsilon_{3/2}=1.89$ MeV, $\epsilon_{1/2}=3.91$ MeV and $\epsilon_{5/2}=6.49$ MeV for FPD6. The two body matrix elements

Table 1

^{48}Ca and ^{56}Ni gaps and single particle energies, with the interactions KB3 and FPD6 (energies in MeV).

	Δ			$\epsilon_{\frac{5}{2}} - \epsilon_{\frac{3}{2}}$			$\epsilon_{\frac{1}{2}} - \epsilon_{\frac{3}{2}}$		
A=48	Exp.	KB3	FPD6	Exp.	KB3	FPD6	Exp.	KB3	FPD6
t=0	4.80	5.25	4.61	3.59	3.53	2.66	2.02	1.70	2.51
Full	4.80	5.17	4.69	3.59	3.80	2.76	2.02	1.81	2.37
A=56	Exp.	KB3	FPD6	Exp.	KB3	FPD6	Exp.	KB3	FPD6
t=0	6.39	8.57	7.41	0.77	0.38	-0.48	1.11	1.15	2.58
t=3	6.39	7.73	6.41	0.77	0.76	0.07	1.11	1.14	1.88

defining FPD6 are scaled with the mass number A as $(42/A)^{0.35}$, while KB3 does not incorporate any mass dependence.

Notice that KB3 does definitely better than FPD6 for the single particle spectra of ^{49}Ca and ^{57}Ni , while for the ^{56}Ni gap, FPD6 is better.

In addition the modification of KB3's gap, we want to make it mass dependent, in order to be able to use it safely around and beyond ^{56}Ni , therefore we have to adjust the monopoles anew. As the gaps are subject to variation when correlations are allowed, some trial and error fitting of the monopole changes is needed. The final modifications of KB3, defining KB3G for A=42 (we stick to the $(42/A)^{1/3}$ mass dependence) are the following:

$$\begin{aligned}
V_{fp}^{T=1}(\text{KB3G}) &= V_{fp}^{T=1}(\text{KB3}) - 50 \text{ keV}, \\
V_{fp}^{T=0}(\text{KB3G}) &= V_{fp}^{T=0}(\text{KB3}) - 100 \text{ keV}, \\
V_{ff_{5/2}}^{T=1}(\text{KB3G}) &= V_{ff_{5/2}}^{T=1}(\text{KB3}) - 100 \text{ keV}, \\
V_{ff_{5/2}}^{T=0}(\text{KB3G}) &= V_{ff_{5/2}}^{T=0}(\text{KB3}) - 150 \text{ keV}, \\
V_{pp}^T(\text{KB3G}) &= V_{pp}^T(\text{KB3}) + 400 \text{ keV},
\end{aligned}$$

where p denotes any of the orbits $2p_{\frac{1}{2}}$ and $2p_{\frac{3}{2}}$.

The T=0 and T=1 modifications are different in order to recover simultaneously the good gaps around ^{48}Ca and ^{56}Ni . The modification of the pp centroids bears no relationship with the gaps, it is aimed to give a single hole spectrum of ^{80}Zr in accord with the predictions of ref [36]. It is important to remark that, for the nuclei already studied with KB3, KB3G produces equivalent results.

Table 2

Same as in table 1 with the modified interactions KB3G and FPD6*.

	Δ			$\epsilon_{\frac{5}{2}} - \epsilon_{\frac{3}{2}}$			$\epsilon_{\frac{1}{2}} - \epsilon_{\frac{3}{2}}$		
A=48	Exp.	KB3G	FPD6*	Exp.	KB3G	FPD6*	Exp.	KB3G	FPD6*
t=0	4.80	4.73	4.61	3.59	3.20	3.04	2.02	1.71	2.13
Full	4.80	4.69	4.68	3.59	3.44	3.10	2.02	1.82	2.03
A=56	Exp.	KB3G	FPD6*	Exp.	KB3G	FPD6*	Exp.	KB3G	FPD6*
t=0	6.39	7.12	7.41	0.77	0.05	0.24	1.11	1.23	1.86
t=3	6.39	6.40	6.45	0.77	0.43	0.68	1.11	1.19	1.45

In the case of FPD6, the gaps are nearly correct and the monopole defects amount to having the $1f_{5/2}$ orbit too low and the $2p_{1/2}$ orbit too high, both in ^{49}Ca and ^{57}Ni . The modifications that repair that are:

$$V_{ff_{5/2}}^{T=0,1}(\text{FPD6}^*) = V_{ff_{5/2}}^{T=0,1}(\text{FPD6}) + 50 \text{ keV},$$

$$V_{fp_{1/2}}^{T=0,1}(\text{FPD6}^*) = V_{fp_{1/2}}^{T=0,1}(\text{FPD6}) - 50 \text{ keV}.$$

In table 2 we present the resulting values around ^{48}Ca and ^{56}Ni . Notice that we have not aimed to an exact agreement. In particular, we know [39] that a t=3 calculations is not fully converged in ^{57}Ni , therefore we have let room for the $1f_{5/2}$ to move up and for the $2p_{1/2}$ to move down a little. We also show the evolution of the quasiparticle neutron gaps through the N=28 isotones for both modified interactions in table 3, The gaps produced by FPD6 do not differ appreciably from those of FPD6*. The agreement with the experimental results is the best that can be reasonably aimed to.

Once the monopole part under control, we can analyse the multipole hamiltonian using the method of ref. [33]. It amounts to diagonalize the monopole-free two body matrix elements in the particle-particle representation or in the particle-hole representation (i.e. after a Racah transformation). In the former case, the physically relevant terms are the isovector and isoscalar pairing terms, while in the latter all the multipoles will show up with different coherent strengths given by the lowest eigenvalues of the respective matrices. In table 4, we have listed these numbers for the two interactions and for the most important multipoles. The differences are small; basically consist in FPD6 being 5-10% more intense than KB3 in all the channels. It is however satisfying the closeness of the values for two effective interactions derived by very different procedures. Remember that for its multipole part, KB3 is just equivalent to the original Kuo and Brown G-matrix [18] including the “bubble” correction,

Table 3

Theoretical quasiparticle neutron gaps of the N=28 isotones (in MeV) compared with experiment. For $Z>23$ we list $t=3$ results, for the rest, full pf -shell results (energies in MeV).

Nucleus	Δ			$\delta = \Delta(exp) - \Delta(th)$	
	FPD6*	EXP.	KB3G	FPD6*	KB3G
^{48}Ca	4.68	4.81	4.70	0.13	0.11
^{49}Sc	4.05	4.07	3.99	0.02	0.08
^{50}Ti	4.66	4.57	4.41	-0.09	0.16
^{51}V	3.61	3.74	3.53	0.13	0.21
^{52}Cr	4.03	4.10	3.76	0.07	0.34
^{53}Mn	3.20	3.12	3.00	-0.08	0.12
^{54}Fe	4.30	4.08	4.02	-0.22	0.06
^{55}Co	4.00	4.01	4.16	0.01	-0.15
^{56}Ni	6.45	6.39	6.41	-0.06	-0.02

Table 4

Strengths (in MeV) of the coherent terms of the multipole Hamiltonian.

Interaction	particle-particle		particle-hole		
	JT=01	JT=10	$\lambda\tau=20$	$\lambda\tau=40$	$\lambda\tau=11$
KB3	-4.75	-4.46	-2.79	-1.39	+2.46
FPD6	-5.06	-5.08	-3.11	-1.67	+3.17
GOGNY	-4.07	-5.74	-3.23	-1.77	+2.46

while FPD6 was obtained via a potential fit to selected energy levels in the pf -shell. This supports the conclusions in [33] about the universality of the multipole shell model Hamiltonian.

We have purposely left to the end the line labeled GOGNY. It comes from the same analysis applied to the pf -shell two body matrix elements obtained using the density dependent interaction of Gogny [40]. The calculation was carried out using the single particle wave function obtained in a spherical Hartree-Fock calculation for ^{48}Cr in the uniform filling approximation in ref. [41]. In spite of the rather hybrid approach, the most important terms are again very similar to those arising from a G-matrix or from a shell model fit. In particular the agreement for the quadrupole and the spin-isospin terms is excellent. When it comes to pairing, this way of looking to the interaction

can help to overcome some language barriers between mean field and shell model practitioners. As it is evident from the table, the Gogny interaction has essentially the same amount of isovector and isoscalar pairing than the realistic interactions. Therefore, it contains the right proton-neutron pairing. Thus, if there is something to blame in the mean field calculations for $N=Z$ nuclei, it should be rather the mean field approximations and not the interaction itself.

In what follows we shall use mainly the interaction KB3G. We will compare in some cases with KB3 in order to evaluate the importance of the changes made in the monopole behaviour. The comparison with FPD6 will show to what extent the residual differences between good behaved interactions can have spectroscopic consequences. We have not attempted to compute all the states not even to draw those we have computed. Those not shown here can be obtained on request to the authors.

3 The isobars $A=50$

We have carried out the full pf -shell calculations for all the isobars. The results for ^{50}Cr and ^{50}Mn have been already published in refs. [16,4,17]. The experimental data for which no specific credit is given are taken from ref. [32].

3.1 Spectroscopy of ^{50}Ca

The experimental data are compared with the calculation in fig. 1. All the experimental states are plotted. We also plot all the calculated ones up to 5 MeV. Beyond, only the yrast states are drawn. The scarcity of spin assignment precludes a more detailed analysis. The 2^+ excitation energy is well reproduced as well as the gap in the spectrum between 1 and 3 MeV of excitation energy. KB3 gives equivalent results. No experimental information on transitions is available.

3.2 Spectroscopy of ^{50}Sc

Figure 2 reflects the experimental situation and our calculated spectrum. We have plotted all the experimental states even if only the lowest ones have assigned spin. All the calculated states up to the first 7^+ state are shown. Above it, only the yrast band. The ground state multiplet, $(1f_{7/2})^9, 2p_{3/2}$ is well reproduced. The first excited state must be a 2^+ because the multiplet cannot contain two 3^+ 's. The triplet at ~ 2 MeV, belonging to the configurations

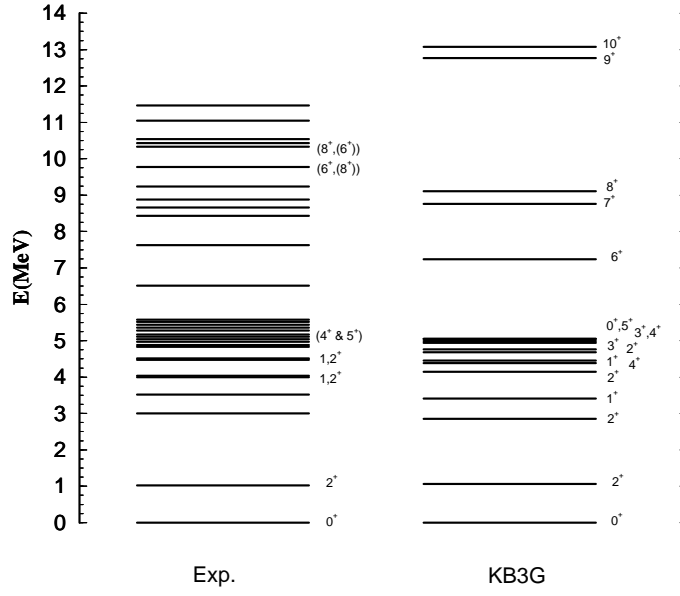


Fig. 1. Energy levels of ^{50}Ca .

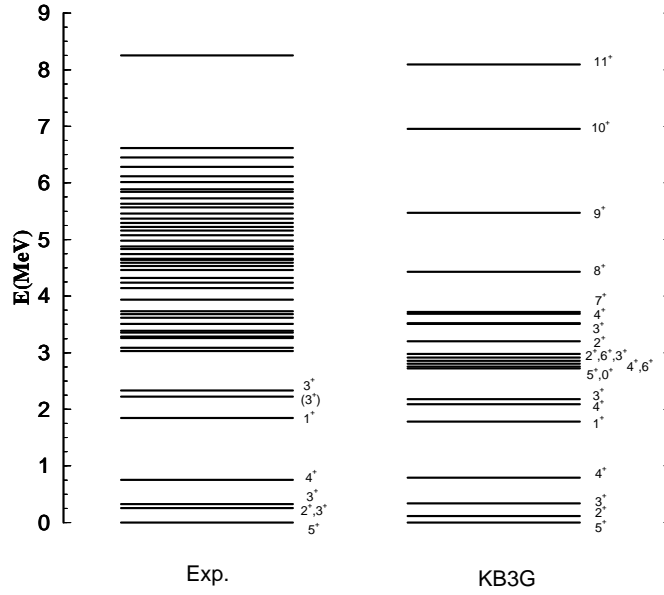


Fig. 2. Energy levels ^{50}Sc .

$(1f_{7/2})^9, (1f_{5/2}, 2p_{1/2})^1$, is also well given. Beyond, the level density increases rapidly and no spin assignments are available. Notice that the experimental density of states is nicely reproduced up to 4 MeV.

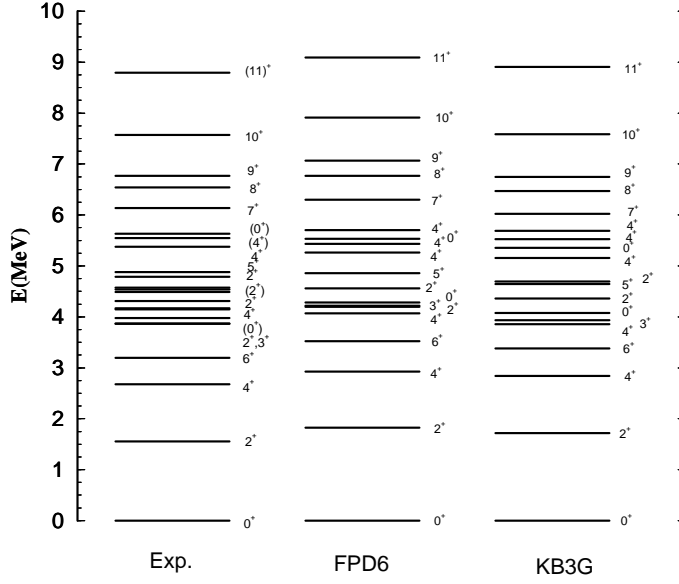


Fig. 3. Energy levels of ^{50}Ti .

3.3 Spectroscopy of ^{50}Ti

^{50}Ti is the stable member of the isobaric multiplet and the best known experimentally. It is semi-magic and therefore any defects in the neutron gap would be evident in the spectrum. In fig 3 the experimental level scheme is compared with the full pf-shell results using the interactions KB3G and FPD6. Up to 4 MeV all the states are plotted. Between 4 MeV and 5.6 MeV only those with unambiguous experimental spin assignment and beyond, only the yrast. The agreement is impressive for the two interactions, perhaps with a bonus for KB3G. Notice the excellent reproduction of the second and third 0^+ states as well as the perfect location of the high spin states. The second 0^+ corresponds to the excitation of two neutrons to the $2p_{3/2}$ orbit, while the third has a more complex structure.

Table 5
Transitions in ^{50}Ti .

$B(E2) (e^2 fm^4)$	Exp.	Th.
$2^+ \rightarrow 0^+$	58(9)	88
$4^+ \rightarrow 2^+$	60(1)	86
$6^+ \rightarrow 4^+$	34(1)	41

The quadrupole and the magnetic moments of the yrast $J = 2^+$ and $J = 6^+$

states are known [42]. Their values, $\mu_{exp}(2^+) = 2.89(15)\mu_N$ [43], $Q_{exp}(2^+) = +8(16) e fm^2$ and $\mu_{exp}(6^+) = +9.3(10)\mu_N$ agree quite well with our predictions; $\mu(2^+) = +2.5\mu_N$, $Q(2^+) = +6 e fm^2$ and $\mu(6^+) = +8.3\mu_N$. A more detailed discussion on the magnetic moments is given in section 8. Similarly the $E2$ transitions of the yrast $J = 2^+, 4^+$ y 6^+ states are well reproduced by the calculation (see table 5).

3.4 Energy levels of ^{50}V

The experimental information is also very rich for this nucleus. Given the high level density, we have represented in fig. 4 all the states up to 1.6 MeV only. Above, just the high spins and a couple of 0^+ 's and 1^+ 's that may have experimental counterparts. The calculation gives a good reproduction of the ground state quintuplet and locates correctly the high spin states 9^+ , 10^+ and 11^+ . The only discrepancy affects to the bunch of 1^+ , 2^+ and 3^+ states at around 1.5 MeV that are placed 500 keV too low.

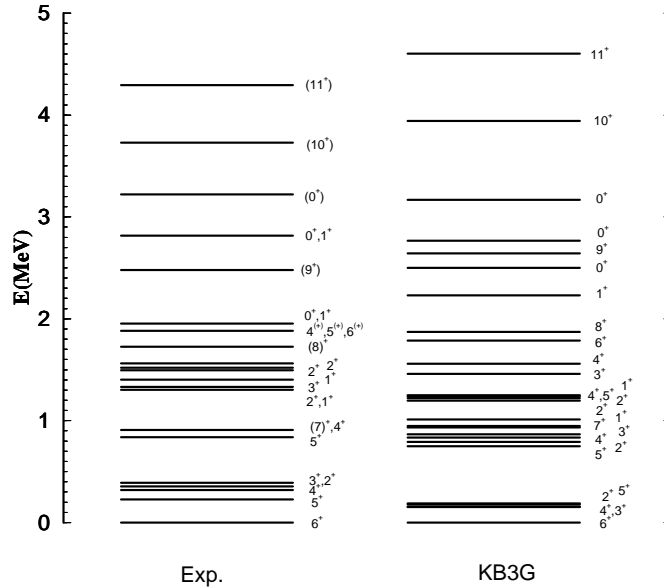


Fig. 4. Energy levels of ^{50}V .

The magnetic and the quadrupole moment of the $J = 6^+$ ground state have been measured [42]. Their values ($\mu_{exp}(6^+) = +3.3456889(14)\mu_N$, $Q_{exp}(6^+) = +20.9(40) e fm^2$) are very well reproduced by the calculations ($\mu(6^+) = +3.18\mu_N$, $Q(6^+) = +19.6 e fm^2$). The electromagnetic transitions of the yrast states are also known (table 6). Notice the excellent agreement found for the -dominant-M1 transitions. For the $\Delta J=1$, E2 transitions the huge error bars make the

comparison meaningless. On the contrary, for the only $\Delta J=2$ transition measured, the agreement is very good.

Table 6
Transitions in ^{50}V .

	Exp.	Th.
$B(M1)$	(μ_N^2)	(μ_N^2)
$7^+ \rightarrow 6^+$	1.2(2)	1.0
$8^+ \rightarrow 7^+$	0.3(1)	0.2
$11^+ \rightarrow 10^+$	0.9(3)	1.1
$B(E2)$	$(e^2 fm^4)$	$(e^2 fm^4)$
$7^+ \rightarrow 6^+$	875^{+1313}_{-875}	108
$8^+ \rightarrow 6^+$	98(44)	74
$8^+ \rightarrow 7^+$	219^{+438}_{-219}	10
$11^+ \rightarrow 10^+$	109^{+328}_{-109}	29

4 The isobars $A=51$

4.1 Spectroscopy of ^{51}Ca

The experimental data become rarer as we go far from stability. In ^{51}Ca only the ground state $J = \frac{3}{2}^-$ is assigned in the experimental scheme. It is what is expected in any reasonable calculation. This nucleus was also studied in ref. [44], using the interactions KB3 and FPD6. As no comparison with the data is possible, we can examine the predictions of the different interactions. In fig. 5 we compare KB3 and KB3G. As the gap is very similar for the two interactions in this nucleus, the differences must be due to the changes in the pp interaction. This is clearly seen in the figure. The four states $3/2^-$, $1/2^-$, $5/2^-$ and $3/2^-$ are dominantly p^3 states and remain unchanged between KB3 and KB3G. However, the states $7/2^-$ and $5/2^-$ are swapped with a relative change of about 2 MeV. This is due to their different structures; the $5/2^-$ is $f_7^8 p^2 f_5$, thus, with KB3G it gains 800 keV relative to the $f_7^8 p^3$ states, the $7/2^-$ has a structure $f_7^7 p^4$ and it loses about 1.2 MeV. Similar arguments explain the lowering of the bunch of states at about 5 MeV excitation energy. Therefore a better experimental spectrum will be of much help in refining these monopolar changes.

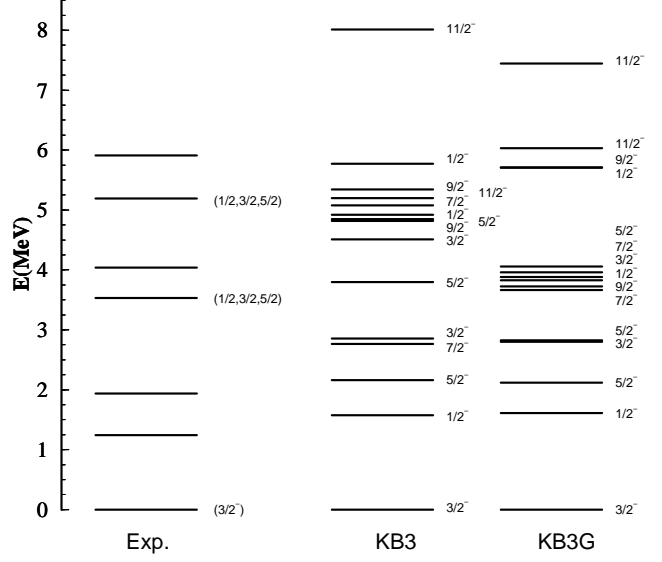


Fig. 5. Energy levels of ^{51}Ca .

4.2 Spectroscopy of ^{51}Sc

As in ^{51}Ca , this nucleus was studied in ref. [44]. Some numerical errors present in this reference were discussed and corrected in refs. [45–47]. Figure 6 shows all the known experimental states. The calculated ones up to 4 MeV energy are also shown. Our results using KB3G are slightly better than those obtained with KB3 and substantially better than those produced by FPD6 [45,47], specially up to 2 MeV of excitation energy where the spacing of the calculated levels follows closely that of the experiment.

4.3 Spectroscopy of ^{51}Ti

In figure 7 we have plotted all the levels up to 3 MeV and a few more up to 4 MeV which have spin and parity assignments. No high spin states are known beyond this energy. The agreement is quite good, exception made of a couple of doublets that come out inverted ($J = \frac{5}{2}^-$ and $J = \frac{7}{2}^-$ at 1.5 MeV and the second $J = \frac{7}{2}^-$ with the first $J = \frac{11}{2}^-$ at around 2.5 MeV). The experimental spin assignment for the state around 3.7 MeV is either $J = \frac{13}{2}^-$ or $J = \frac{17}{2}^-$. Our calculation predicts a $J = \frac{13}{2}^-$ close to this energy, while the first $J = \frac{17}{2}^-$ state is predicted 2 MeV higher. If we compute the ^{51}Ti spectrum with FPD6 there are not significant differences, because the dominant configurations are $(f_{\frac{7}{2}}^8 p_{\frac{3}{2}}^1)_\nu (f_{\frac{7}{2}}^2)_\pi$, therefore the $f_{\frac{5}{2}}$ does not play an

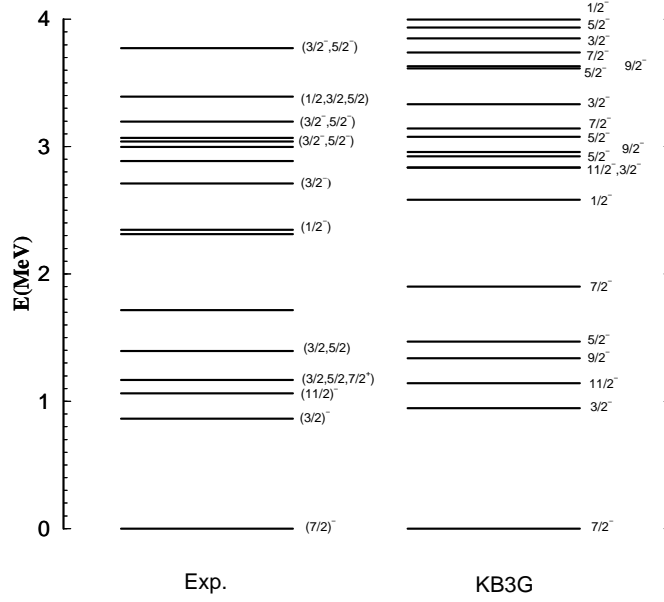


Fig. 6. Energy levels of ^{51}Sc .

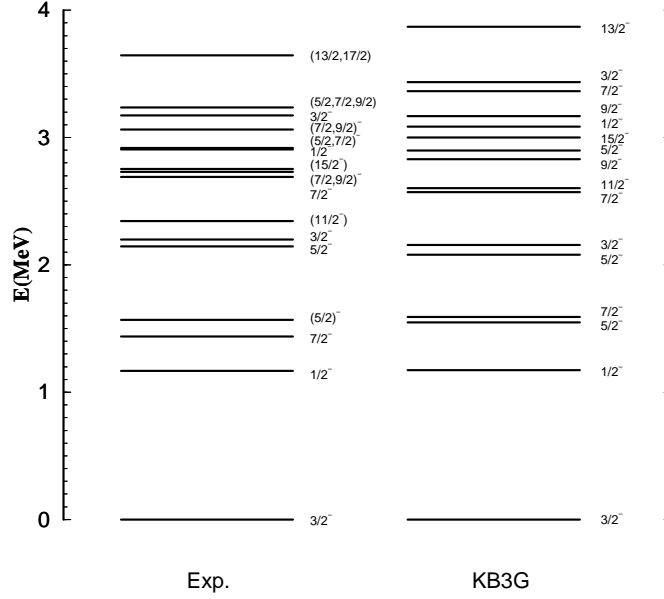


Fig. 7. Energy levels of ^{51}Ti .

important role. We can interpret most of the ^{51}Ti level scheme as the result of the coupling $^{50}\text{Ti} \otimes p_{3/2}^1$.

Some electromagnetic transitions are experimentally known that are well reproduced by the calculation (see table 7). Again in this case, the E2 transitions

with $\Delta J=1$ are poorly determined experimentally, due to the dominance of the M1 transitions. The calculated $\Delta J=2$ B(E2)'s agree extremely well with the measured values.

Table 7

Transitions in ^{51}Ti .

	Exp.	Th.
$B(M1)$	(μ_N^2)	(μ_N^2)
$\frac{5}{2}^- \rightarrow \frac{3}{2}^-$	0.06(2)	0.07
$B(E2)$	$(e^2 fm^4)$	$(e^2 fm^4)$
$\frac{5}{2}^- \rightarrow \frac{3}{2}^-$	348(112)	88
$\frac{7}{2}^- \rightarrow \frac{3}{2}^-$	225(202)	88
$\frac{11}{2}^- \rightarrow \frac{7}{2}^-$	95(17)	95
$\frac{15}{2}^- \rightarrow \frac{11}{2}^-$	62(24)	53

4.4 Spectroscopy of ^{51}V

^{51}V is the stable isotope in the isobar chain $A = 51$ and corresponds to the $N=28$ neutron shell closure. The experimental information is very rich, extending up to 13 MeV. Figure 8 shows the experimental yrast band with all the known high spin assignments compared with the calculated one including three more predicted spins. The agreement is extremely good. For a more complete analysis below 3 MeV energy, where more experimental information is available, we have plotted in figure 9 all the levels up to that energy and a few more above that can be put in correspondence with the experiment. We have calculated with KB3G and FPD6, both reproduce nicely the level scheme but definitely the quality of the agreement with KB3G is better. The magnetic moments of the ground state $J = \frac{7}{2}^-$ and first excited state $J = \frac{5}{2}^-$ as well as the quadrupole moment of the ground state are known [42]. Their values are:

$$\begin{aligned}\mu_{exp}(\frac{7}{2}^-) &= +5.14870573(18) \mu_N & Q_{exp}(\frac{7}{2}^-) &= -5.2(10) e fm^2 \\ \mu_{exp}(\frac{5}{2}^-) &= +3.86(33) \mu_N\end{aligned}$$

while the calculation gives:

$$\begin{aligned}\mu(\frac{7}{2}^-) &= +4.99 \mu_N & Q(\frac{7}{2}^-) &= -6.5 e fm^2 \\ \mu(\frac{5}{2}^-) &= +3.36 \mu_N\end{aligned}$$

Table 8
Transitions in ^{51}V .

	Exp.	Th.
$B(M1)$	(μ_N^2)	(μ_N^2)
$\frac{9}{2}^- \rightarrow \frac{7}{2}^-$	0.0006(2)	$0.2 \cdot 10^{-6}$
$\frac{13}{2}^- \rightarrow \frac{11}{2}^-$	< 0.0077	0.014
$B(E2)$	$(e^2 fm^4)$	$(e^2 fm^4)$
$\frac{9}{2}^- \rightarrow \frac{7}{2}^-$	35(6)	32
$\frac{11}{2}^- \rightarrow \frac{7}{2}^-$	95(8)	103
$\frac{13}{2}^- \rightarrow \frac{11}{2}^-$	< 34.8	0.01
$\frac{15}{2}^- \rightarrow \frac{11}{2}^-$	66(6)	78

4.5 Spectroscopy of ^{51}Cr

We present in fig. 10 the results for the yrast band of ^{51}Cr in a $t = 5$ truncation and in the full space using KB3G. We have also included the low-lying $J = \frac{1}{2}^-, \frac{3}{2}^-$ and $\frac{5}{2}^-$ states, and a second state of each spin from $J = \frac{19}{2}^-$ on. The figure shows that the full calculation do not modify substantially the results obtained at $t = 5$. The agreement with the experimental data is very

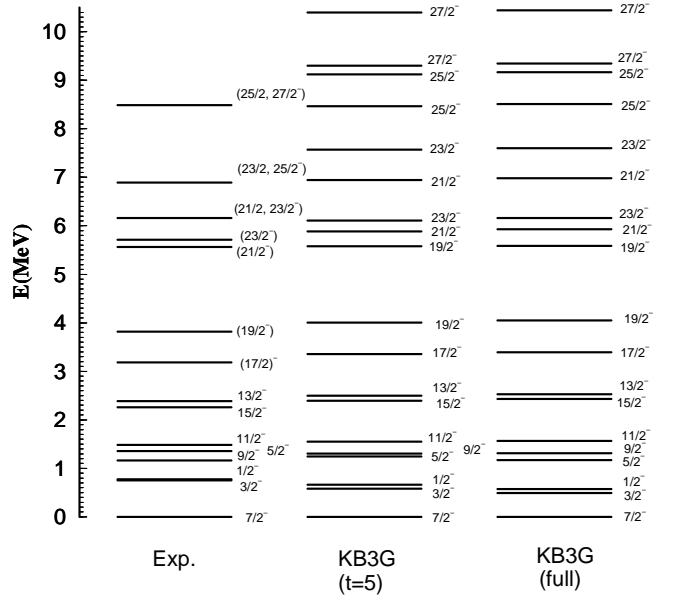


Fig. 10. Yrast band of ^{51}Cr ; experiment, $t = 5$ and full calculation.

satisfactory. Notice that our prediction for the spins of the triplet of states around 6 MeV is shifted down by one unit relative to the preliminary experimental assignment, that should be revised in the light of our results. The detailed comparison with all the levels up to 2.8 MeV, and with the high spin states above this energy up to $J = \frac{19}{2}^-$ is carried out with a $t = 5$ calculation. The results for both KB3 and KB3G are plotted in figure 11.

The agreement is very good in spite of some local inversions. We can also notice that KB3G improves systematically the KB3 results. The sequence of states $J = \frac{7}{2}^-, \frac{9}{2}^-, J = \frac{11}{2}^-$ belong to the configuration $(1f_{7/2})^{11}$, while the doublets $J = \frac{3}{2}^-, \frac{1}{2}^-$ and $J = \frac{5}{2}^-, \frac{7}{2}^-$ located at 800 keV and 1.5 MeV, correspond to a neutron jump to the orbit $2p_{3/2}$, a sort of coupling $^{50}\text{Cr} \otimes p_{3/2}^1$. As a consequence of the reduction of the gap, KB3G put these doublets at lower energy, while leaving the yrast ones unchanged. This provides a good illustration of a direct monopole effect. A similar though more pronounced effect is seen in the lowering of the doublet $J = \frac{3}{2}^-, \frac{5}{2}^-$ experimentally at 2 MeV predicted by KB3 500 keV too high, again a gap effect solved by KB3G. Besides, the high spin states were also too high in KB3 and come now very close to their experimental position.

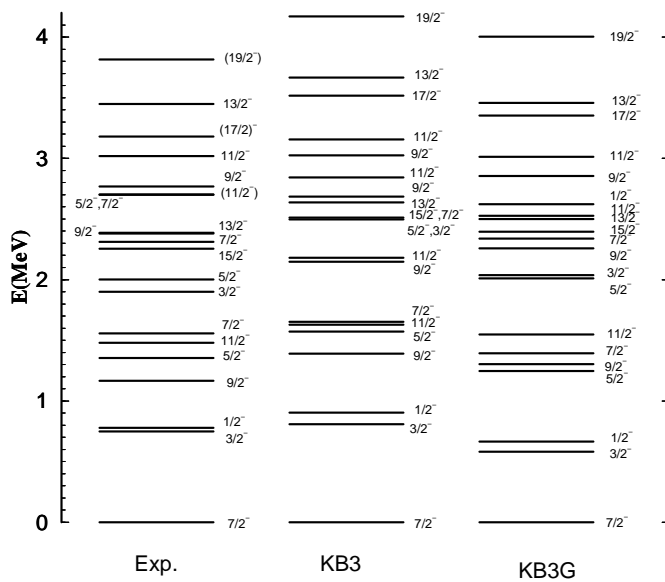


Fig. 11. Energy levels of ^{51}Cr , $t = 5$.

The magnetic moments of the ground state and the first excited state are known, $(\mu_{exp}(\frac{7}{2}^-) = -0.934(5) \mu_N$ and $\mu_{exp}(\frac{3}{2}^-) = -0.86(12) \mu_N$). Our prediction for the ground state is quite accurate $\mu(\frac{7}{2}^-) = -0.886 \mu_N$ while for the $J = \frac{3}{2}^-$ state our result $\mu(\frac{3}{2}^-) = -0.40 \mu_N$ is off by a factor two.

In table 9 we compare the experimental and calculated transition probabilities. The $B(M1)$'s and the $\Delta J=2$ $B(E2)$'s are well reproduced. However this is not the case for the $\Delta J=1$ $B(E2)$'s, in particular the discrepancies are huge for the transitions $\frac{11}{2}^- \rightarrow \frac{9}{2}^-$ and $\frac{13}{2}^- \rightarrow \frac{11}{2}^-$. We have carried out a consistency test using the experimental $M1/E2$ branchings, δ , and we have found that the experimental δ values are inconsistent with the experimental $B(E2)$'s but consistent with the calculated values. This is not surprising, because of the complete dominance of the $M1$ transition, that may cause large errors in the extraction of the $B(E2)$ value. In order to discard any other origin of the discrepancy we have repeated the calculation with FPD6 and the situation is the same or even worse.

Table 9
Transitions in ^{51}Cr .

	Exp.	Th.
$B(M1)$	(μ_N^2)	(μ_N^2)
$\frac{9}{2}^- \rightarrow \frac{7}{2}^-$	0.31683(3043)	0.439
$\frac{11}{2}^- \rightarrow \frac{9}{2}^-$	1.253(537)	1.295
$\frac{13}{2}^- \rightarrow \frac{11}{2}^-$	0.8950(1969)	1.356
$B(E2)$	$(e^2 fm^4)$	$(e^2 fm^4)$
$\frac{9}{2}^- \rightarrow \frac{7}{2}^-$	124(56)	213
$\frac{11}{2}^- \rightarrow \frac{7}{2}^-$	67(34)	72
$\frac{11}{2}^- \rightarrow \frac{9}{2}^-$	8(3)	180
$\frac{13}{2}^- \rightarrow \frac{11}{2}^-$	6(1)	151
$\frac{15}{2}^- \rightarrow \frac{11}{2}^-$	44(1)	53

4.6 Spectroscopy of ^{51}Mn

As for ^{51}Cr , we present in fig. 12 the comparison between the experimental level scheme and our calculations in the full space and with a $t = 5$ truncation for the yrast band and the $\frac{1}{2}^-$, $\frac{3}{2}^-$ doublet around 2 MeV. Again no relevant difference is appreciated between both calculated schemes and the agreement with the experiment is very good. Therefore, a $t = 5$ truncation is used to get a more detailed spectroscopy for all the states below 3 MeV and for the high spins up to $J = \frac{19}{2}^-$ (fig. 13). New data are available from a Gammasphere experiment aimed to the study of Coulomb energy differences in mirror nuclei [48]. The agreement is very good in both regions, although the high spin states are slightly shifted up.

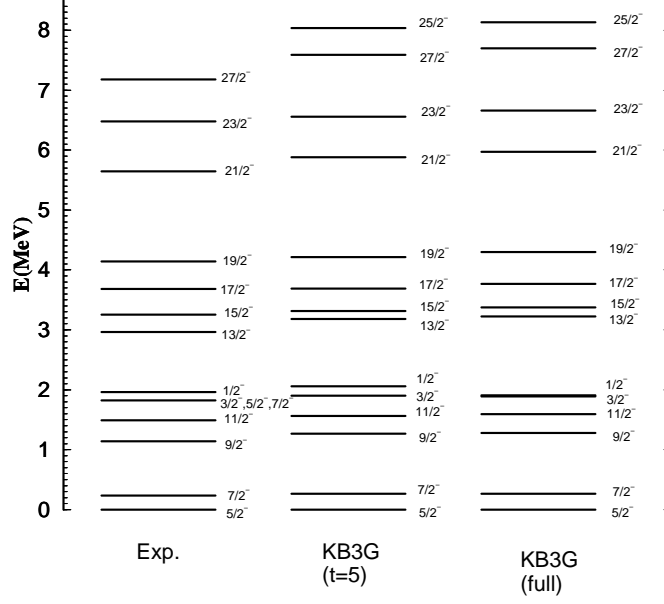


Fig. 12. Yrast band of ^{51}Mn ; experiment, $t = 5$ and full calculation.

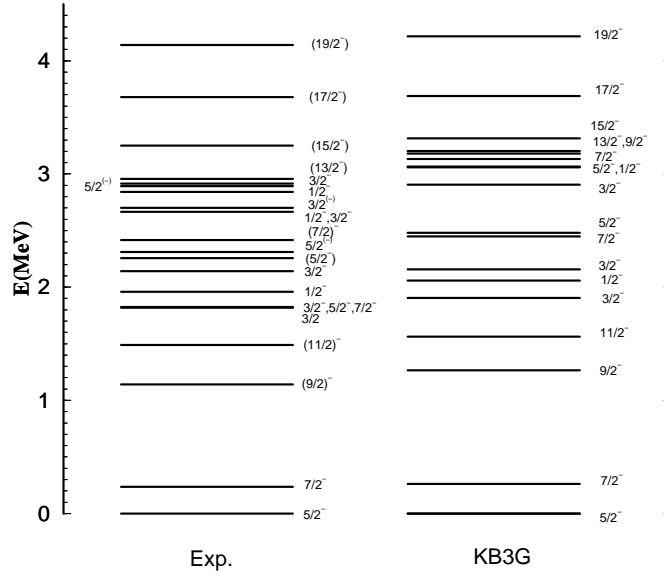


Fig. 13. Energy levels of ^{51}Mn , $t = 5$.

Good agreement is also obtained for the electromagnetic moments of the ground state. The experimental values:

$$\mu_{exp}\left(\frac{5}{2}^{-}\right) = 3.5683(13) \mu_N$$

$$Q_{exp}\left(\frac{5}{2}^{-}\right) = 42(7) e fm^2$$

are very well reproduced by the KB3G calculation:

$$\begin{aligned}\mu(\tfrac{5}{2}^-) &= 3.40 \mu_N \\ Q(\tfrac{5}{2}^-) &= 35 e fm^2\end{aligned}$$

In addition, there is experimental information on electromagnetic transitions, that we compare with the calculation in table 10. The accord is excellent for the M1 transitions. For the E2's the situation is similar to the other isobars; for the $\Delta J=2$ transitions the agreement is quite good, while some discrepancies are present in the $\Delta J=1$ cases, that can be very large, for instance in the transition from $J = \frac{11}{2}^-$ to $J = \frac{9}{2}^-$. As in the ^{51}Cr case, we have found an inconsistency between the experimental values for the B(M1) and B(E2) and the experimental mixing parameter δ . On the contrary the experimental value is fully compatible with the computed transition probabilities. Notice the abrupt change (more than two orders of magnitude decrease) in the transition probabilities either M1 or E2 of the $J = \frac{17}{2}^-$ state, that are spectacularly reproduced by the calculation. A very intuitive physical explanation of this isomerism will be given later, when discussing the Coulomb energy differences between the yrast states of the mirror pair ^{51}Fe - ^{51}Mn .

Table 10
Transitions in ^{51}Mn .

	Exp.	Th.
$B(M1)$	(μ_N^2)	(μ_N^2)
$\frac{7}{2}^- \rightarrow \frac{5}{2}^-$	0.207(34)	0.177
$\frac{9}{2}^- \rightarrow \frac{7}{2}^-$	0.16(5)	0.114
$\frac{11}{2}^- \rightarrow \frac{9}{2}^-$	0.6623(2148)	0.423
$\frac{17}{2}^- \rightarrow \frac{15}{2}^-$	0.00012(4)	0.00003
$\frac{19}{2}^- \rightarrow \frac{17}{2}^-$	>0.5728	0.801
$B(E2)$	$(e^2 fm^4)$	$(e^2 fm^4)$
$\frac{7}{2}^- \rightarrow \frac{5}{2}^-$	528(146)	305
$\frac{9}{2}^- \rightarrow \frac{5}{2}^-$	169(67)	84
$\frac{9}{2}^- \rightarrow \frac{7}{2}^-$	303(112)	204
$\frac{11}{2}^- \rightarrow \frac{7}{2}^-$	236(67)	154
$\frac{11}{2}^- \rightarrow \frac{9}{2}^-$	4.16(135)	190
$\frac{17}{2}^- \rightarrow \frac{13}{2}^-$	1.236(337)	2.215

5 The isobars $A=52$

As in the $A = 51$ isobaric multiplet we have performed full $0\hbar\omega$ calculations for all the isotopes in ^{52}Cr and ^{52}Mn the full calculation is limited to the yrast levels. More detailed spectroscopy is carried out with a $t=5$ truncation. The results of the full pf -shell calculation for ^{52}Fe have been already published in [5]. The experimental values are taken from ref. [32].

5.1 Spectroscopy of ^{52}Ca

The experimental information is scarce, as can be seen in figure 14. Both KB3 and KB3G give the same excitation energy for the doublet $J = 1^+, 2^+$ at 2.5 MeV, and reproduce correctly the energy of the first excited state $J = 2^+$. The states whose leading configuration has four p -particles behave like the ground state under the KB3G changes, therefore we expect that their excitation energies do not change between KB3 and KB3G. This is the case for the above mentioned doublet, whose leading configuration is $f_{\frac{7}{2}}^8 p_{\frac{3}{2}}^3 p_{\frac{1}{2}}^1$ and for the second 0^+ whose configuration is $f_{\frac{7}{2}}^8 p_{\frac{3}{2}}^2 p_{\frac{1}{2}}^2$, therefore, both interactions locate them at the same place.

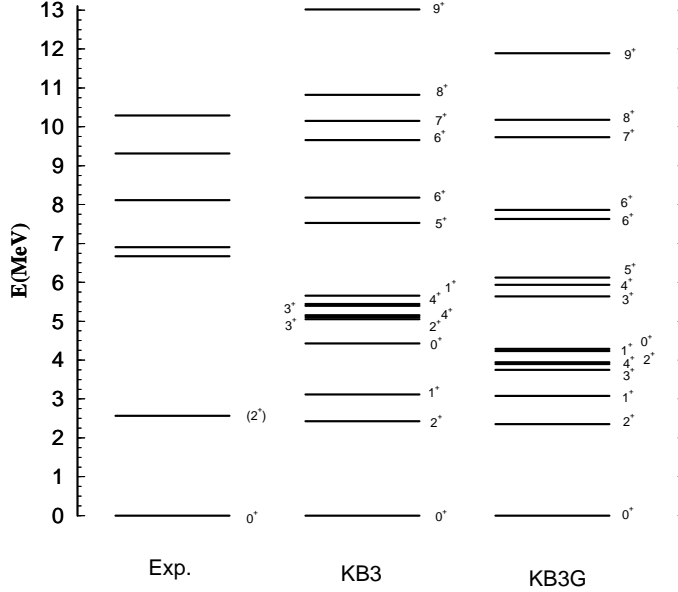


Fig. 14. Energy levels of ^{52}Ca .

The multiplet $J = 1^+, 2^+, 3^+, 4^+$ predicted at 5 MeV by KB3 has a configuration $f_{\frac{7}{2}}^8 p_{\frac{3}{2}}^3 f_{\frac{5}{2}}^1$, consequently it is less affected by the monopole corrections

(ΔV_{pp}) made in KB3G than the ground state, and moves down 1 MeV in excitation energy. The states $J = 5^+$, $J = 6_2^+$, $J = 7^+$, $J = 8^+$ and $J = 9^+$ are also lowered by KB3G, due to the occupation of the $1f_{\frac{5}{2}}^1$ orbit.

5.2 Spectroscopy of ^{52}Sc

The dominant configuration in the ground state of ^{52}Sc is $(f_{\frac{7}{2}}^1)_\pi(f_{\frac{7}{2}}^8 p_{\frac{3}{2}}^3)_\nu$. It produces the multiplet of states with J going from 2^+ to 5^+ , below 1 MeV. Experimentally little is known, the ground state 3^+ , one state without spin assigned at about 0.6 MeV and four 1^+ states seen in the beta decay of ^{52}Ca [49] (see fig. 15). In the figure we include the calculated ground state multiplet and the high spins up to $J = 8^+$, as well as all the $J = 1^+$ states present below 4.5 MeV. According to the KB3G results, the state at 0.6 MeV should be the 2^+ member of the ground state multiplet. In ref. [50] it is argued that this state could be a 1^+ , based on the FPD6 results. However this has to be attributed to the fact that FPD6 puts the $1f_{\frac{5}{2}}$ orbit too low at $N=28$. If this state were a 1^+ , it would have been seen in the decay of ^{52}Ca , and this is not the case. The calculation produces six 1^+ states in the region where experimentally only four have been found. We will discuss the decay pattern of ^{52}Ca in section 6.3.

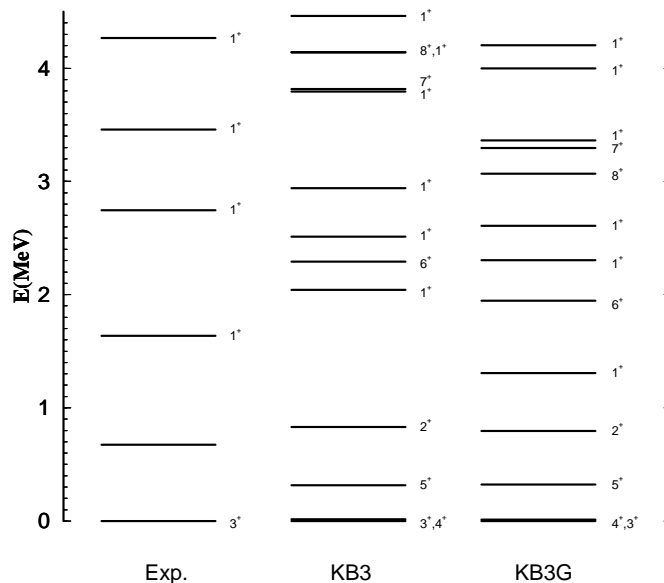


Fig. 15. Energy levels of ^{52}Sc .

5.3 Spectroscopy of ^{52}Ti

The experimental level scheme is compared in figure 16 with the full pf-shell results using the interactions KB3G and FPD6. The location of the yrast states from $J = 0^+$ to $J = 6^+$ corresponding to the dominant configuration $(f_{\frac{7}{2}}^8 p_{\frac{3}{2}}^2)_{\nu} (f_{\frac{7}{2}}^2)_{\pi}$ is correct for both interactions. The lowest states of ^{52}Ti can be described essentially in terms of the coupling $^{50}\text{Ti} \otimes p_{\frac{3}{2}}^2$. Notice the right position of the triplet $J = 2^+, 4^+, 2^+$ at $\sim 2.4 \text{ MeV}$. However, the doublet $J = 4^+, 2^+$ at $\sim 3.5 \text{ MeV}$ is clearly better placed by KB3G than by FPD6.

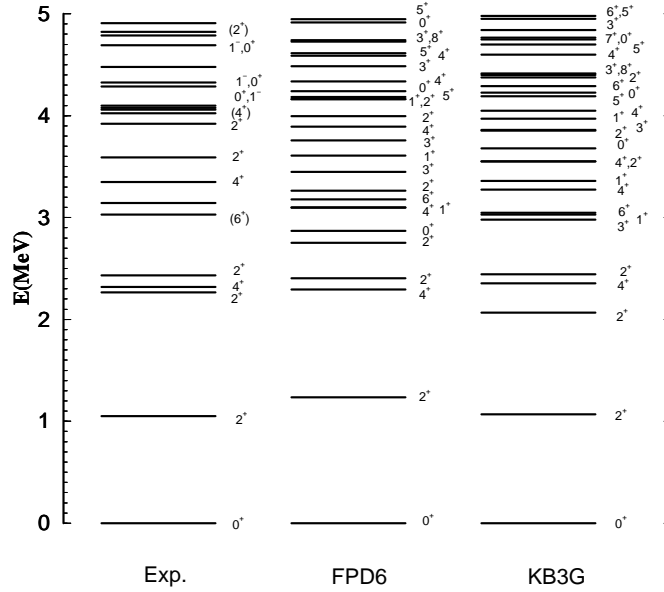


Fig. 16. Energy levels of ^{52}Ti .

These states are dominantly $f_{\frac{7}{2}}^8 f_{\frac{5}{2}}^2$ and they are shifted down by FPD6. This is even more evident for the second $J = 0^+$ state that is reasonably positioned by KB3G but strongly shifted down by FPD6. The richness of the calculated level scheme calls for an improvement of the experimental spectrum.

There are six experimental transitions known [42], though with large uncertainties. The calculated values are in accord with the data, as can be seen in table 11.

Table 11
Transitions in ^{52}Ti .

	Exp.	Th.
$B(M1)$	(μ_N^2)	(μ_N^2)
$2_2^+ \rightarrow 2_1^+$	$0.55^{+0.41}_{-0.25}$	0.85
$2_3^+ \rightarrow 2_1^+$	>0.16	0.51
$B(E2)$	$(e^2 fm^4)$	$(e^2 fm^4)$
$2_1^+ \rightarrow 0^+$	138^{+104}_{-92}	85
$2_2^+ \rightarrow 0^+$	31^{+23}_{-14}	16
$2_3^+ \rightarrow 2_1^+$	>127	66
$6^+ \rightarrow 4^+$	$123(22)$	80

5.4 Spectroscopy of ^{52}V

In figure 17 we have plotted all the states with parity and spin assignments up to 2 MeV. Above this energy only the levels with spins equal or greater than 6^+ are shown. The situation is similar to ^{52}Sc . The dominant configuration $(f_{7/2}^3)_\pi(f_{7/2}^8 p_{3/2}^1)_\nu$ in the ground state produces the multiplet of states with J going from 1^+ to 5^+ .

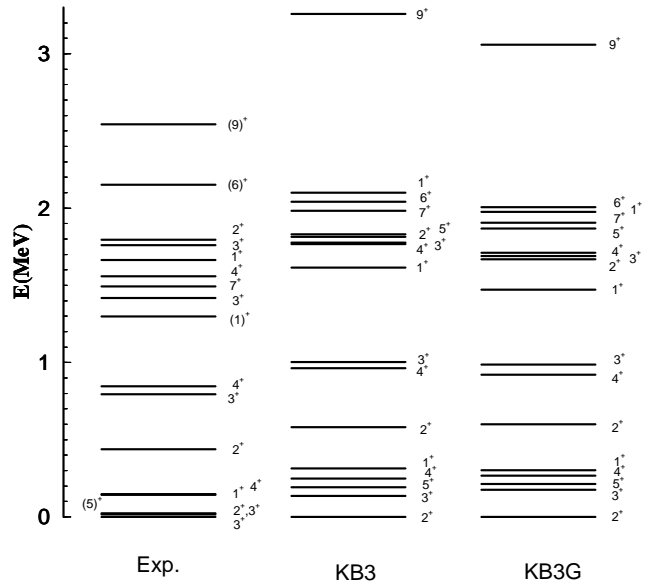


Fig. 17. Energy levels of ^{52}V .

The calculated ground state multiplet is more dilated than its experimental counterpart. Although the more relevant features are well accounted for we do not predict the correct ground state spin. The $J = 3^+, 4^+$ doublet around 850 keV comes out inverted. These states can be described as the result of the coupling $^{51}\text{V} \otimes p_{\frac{3}{2}}^1$. The high spin states $J = 7^+$ and $J = 9^+$ are shifted up, making the agreement with experiment worse than in the other nuclei studied in this work.

Only two electromagnetic transitions are experimentally known [42]: the E2 connecting the states $J = 9^+$ and $J = 7^+$ ($B(E2) = 81(6) e^2 fm^4$) and the M1 connecting the first excited $J = 2^+$ state and the $J = 3^+$ ground state ($B(M1) = 1.7(4) \mu_N^2$). For the first one the calculation produces a value $B(E2) = 87 e^2 fm^4$ and for the second $B(M1, 2^+ \rightarrow 3^+) = 1.7 \mu_N^2$, a rather impressive agreement.

5.5 Spectroscopy of ^{52}Cr

Figure 18 shows the yrast states of ^{52}Cr , up to the band termination, calculated in the full pf -shell and in a $t = 5$ truncation, compared with the experimental values. It is quite evident that the states obtained with a $t = 5$ truncation are nearly converged. The accord of the KB3G results with the experiment is excellent.

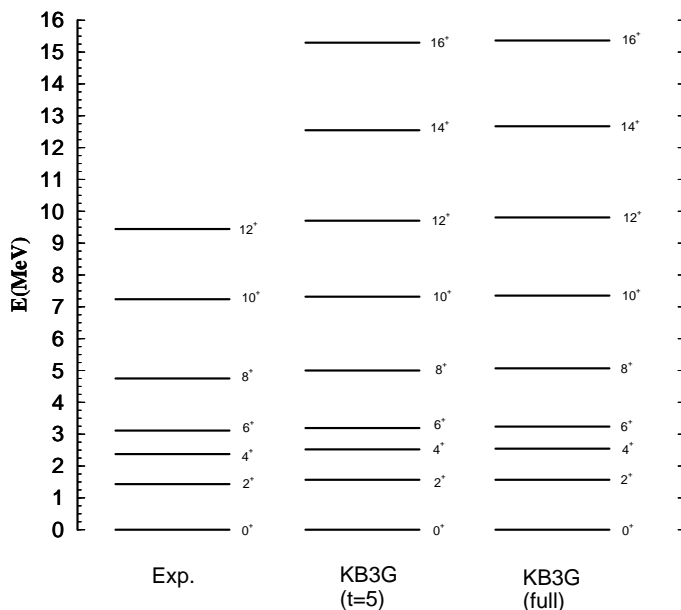


Fig. 18. Yrast band of ^{52}Cr ; experiment, $t = 5$ and full calculation.

More detailed spectroscopic results are shown in figures 19 and 20 in a $t = 5$

truncated calculation. In fig. 19 all the states experimentally known up to ~ 4 MeV [32] have been included as well as the corresponding ones obtained with KB3G and KB3. The levels above this energy are plotted in figure 20, where the experimental data come from a recent experiment [51]. The agreement for the non yrast states is also very satisfactory. Notice the good positioning of the doublets $J = 0^+, 4^+$ at 2.7 MeV and $J = 4^+, 3^+$ at 3.5 MeV and the one to one correspondence between the three $J = 2^+$ and the three $J = 5^+$ states measured in the excitation energy range 3 MeV \sim 4 MeV and the calculated ones. Beyond 4 MeV the yrare states and the odd yrast are also fairly well accounted for. It is clear from fig. 20 that KB3G produces a more satisfactory level scheme than KB3, that shifts up all the levels with spins greater than $J = 8^+$, the maximum value attainable within the $(1f_{7/2})^{12}$ configuration. This is again a manifestation of the too large N=28 gap produced by this interaction.

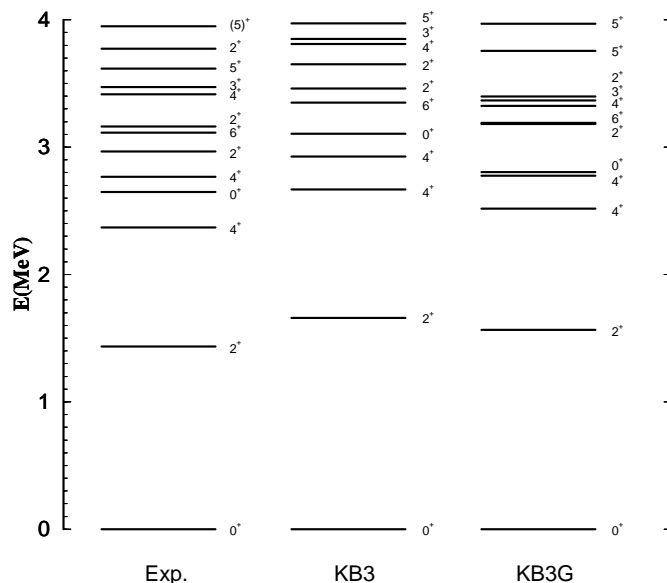


Fig. 19. Energy levels of ^{52}Cr up to 4 MeV, $t = 5$.

The experimental magnetic and quadrupole moments for the first excited state $J = 2^+$ are:

$$\begin{aligned}\mu_{exp}(2^+) &= +3.00(50) \mu_N \\ Q_{exp}(2^+) &= -8.2(16) e fm^2\end{aligned}$$

and the calculated ones:

$$\begin{aligned}\mu(2^+) &= +2.50 \mu_N \\ Q(2^+) &= -9.4 e fm^2\end{aligned}$$

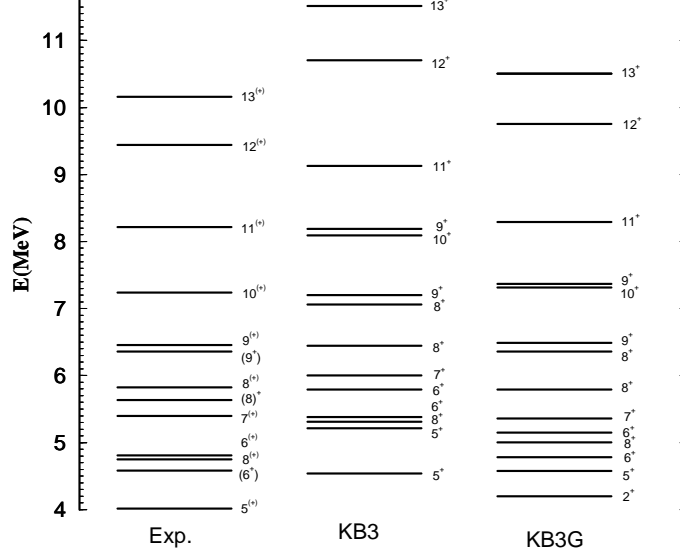


Fig. 20. Energy levels of ^{52}Cr above 4 MeV, $t = 5$.

In table 12 the known experimental values for the electromagnetic transitions between the states of the yrast sequence are given. The correspondence with the predicted ones is good with the exception of the E2 transition $J = 4^+$ to $J = 2^+$, whose measured value is far outside the range expected in this mass region. Given its very large error bar, we would rather disregard this measure.

Table 12
Transitions in ^{52}Cr .

	Exp.	Th.
$B(M1)$	(μ_N^2)	(μ_N^2)
$9^+ \rightarrow 8^+$	0.05728(3759)	0.040
$B(E2)$	$(e^2 fm^4)$	$(e^2 fm^4)$
$2^+ \rightarrow 0^+$	131(6)	132
$3^+ \rightarrow 2^+$	7_{-5}^{+7}	5
$4^+ \rightarrow 2^+$	761(265)	107
$6^+ \rightarrow 4^+$	59(2)	68
$8^+ \rightarrow 6^+$	75(24)	84
$9^+ \rightarrow 8^+$	0.5(20)	0.6

5.6 Spectroscopy of ^{52}Mn

The full space calculation for the yrast states of the odd-odd nucleus ^{52}Mn produces only minor differences with the $t = 5$ results (fig. 21). Notice the full correspondence between the states of the multiplet below 1 MeV. The experimental data for the spins beyond the band termination (11^+ to 16^+) come from a recent experiment [52]. The agreement between experiment and theory is spectacular. There is only three experimental states with spin assignment not represented in the figure: a second $J = (5^+)$ at 1.42 MeV, a third $J = (5^+)$ at 1.68 MeV and a second $J = (6^+)$ at 1.96 MeV. The $t = 5$ calculation places the second $J = 5^+$ at 1.47 MeV, the third $J = 5^+$ at 2.05 MeV and the second $J = 6^+$ at 1.91 MeV.

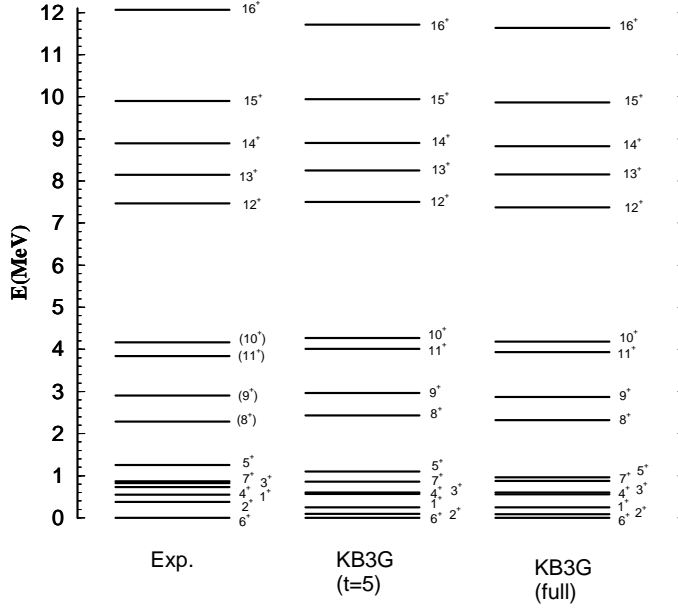


Fig. 21. Yrast band of ^{52}Mn ; experiment, $t = 5$ and full calculation.

The experimental magnetic and quadrupole moments for the ground state are known:

$$\begin{aligned}\mu_{exp}(6^+) &= +3.0622(12) \mu_N \\ Q_{exp}(6^+) &= +50(7) e fm^2\end{aligned}$$

the calculated values reproduce nicely these values:

$$\begin{aligned}\mu(6^+) &= +2.9518 \mu_N \\ Q(6^+) &= +50 e fm^2\end{aligned}$$

Some electromagnetic transitions along the yrast sequence have been measured. The calculations are in fair agreement with them (see table 13).

Table 13
Transitions in ^{52}Mn .

	Exp.	Th.
$B(M1)$	(μ_N^2)	(μ_N^2)
$7^+ \rightarrow 6^+$	0.5012(2506)	0.667
$8^+ \rightarrow 7^+$	>0.015931	0.405
$9^+ \rightarrow 8^+$	$1.074^{+3.043}_{-0.537}$	0.759
$B(E2)$	$(e^2 fm^4)$	$(e^2 fm^4)$
$7^+ \rightarrow 6^+$	92^{+484}_{-81}	126
$8^+ \rightarrow 6^+$	>1.15	33
$8^+ \rightarrow 7^+$	>4.15	126
$9^+ \rightarrow 7^+$	104^{+300}_{-46}	66
$11^+ \rightarrow 9^+$	54(6)	53

6 Half-lives and other β -decay properties

Once the level schemes have been analysed, we study the β^- decays of these nuclei, to complete the description of this mass region. We present the results with the same ordering used for the level schemes. Because of the increasing sizes of the calculations we have limited this study to the isotopes of Calcium, Scandium, Titanium and Vanadium. The calculated values for KB3 and KB3G gathered in the tables correspond to full $0\hbar\omega$ calculation unless otherwise indicated. The Q_{β^-} values are also included. The errors attached to the calculated values proceed from the errors in the experimental Q_{β^-} values. We compute the half-lives by making the convolution of the strength function produced by the Lanczos method with the Fermi function, increasing the number of iterations until convergence is achieved.

6.1 β^- decays in the isobar chain $A = 50$

The experimental and calculated half-lives in the isobar chain $A = 50$ are given in table 14. The agreement is quite satisfactory.

Table 14

Half-lives of $A = 50$ isobars. Q_{β^-} values from [32].

A	J^π	$T_{\frac{1}{2}}$			$Q_{\beta^-}^{exp} (MeV)$
		KB3	KB3G	Exp.	
^{50}Ca	0^+	$11.1^{+0.3}_{-0.2} s$	$11.2^{+0.3}_{-0.3} s$	$13.9(6) s$	$4.966(17)$
			$12.3 \pm 0.3 s$		
^{50}Sc	5^+	$130^{+3}_{-3} s$	$140^{+3}_{-1} s$	$102.5(5) s$	$6.888(16)$
			$120^{+2}_{-1} s$		
^{50}Ti			Stable		
^{50}V			4^{th} forbidden C.E.		

The Gamow-Teller strength function for ^{50}Ca is shown in fig. 22. The amount of strength below the Q_{β^-} value is very small and it is concentrated at ~ 2 MeV. Notice that there is a large amount of strength close above the Q_{β^-} -threshold. Thus, small variations in the excitation energies of the daughter states could influence (although not drastically) the final value of the half-life. In ^{50}Sc (see figure 23) the situation is similar. Only a tiny fraction of the total strength lies below the Q_{β^-} value.

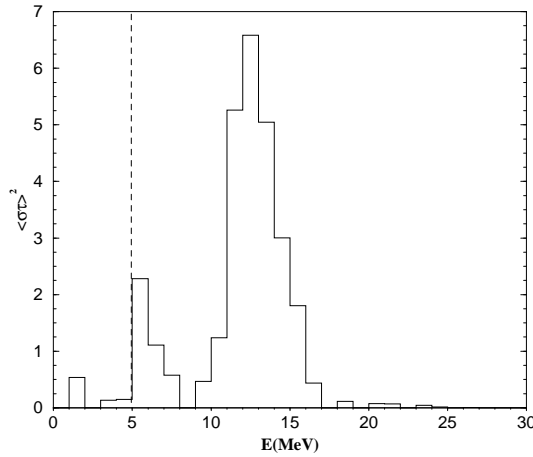


Fig. 22. Gamow-Teller strength after 50 iterations for the ^{50}Ca β^- decay. The $\langle \sigma \tau \rangle^2$ values are summed up in 1 MeV bins. The dashed line indicates the experimental Q_{β^-} value.

We have computed the intensity (in percentage) of the ground state decay to the levels within the Q_{β^-} window of the daughter nucleus. ^{50}Ca decays 99.7% to the excited state $J = 1^+$ at 1.78 MeV in ^{50}Sc , what agrees perfectly with the experimental situation (99.0(13)% decay to the $J = 1^+$ state at 1.85 MeV).

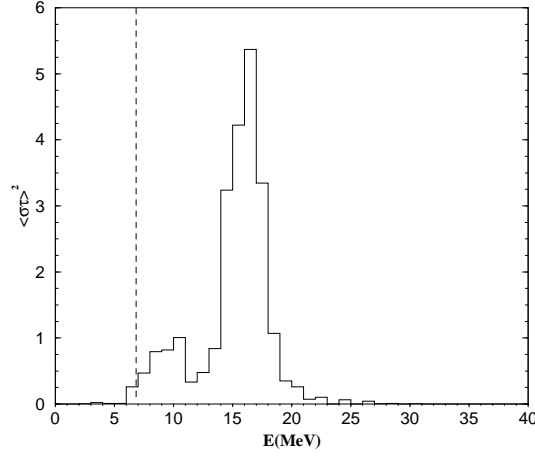


Fig. 23. Gamow-Teller strength after 50 iterations for the ^{50}Sc β^- decay. The $\langle \sigma \tau \rangle^2$ values are summed up in 1 MeV bins. The dashed line indicates the experimental Q_{β^-} value.

Analogously, figure 24 shows the experimental and calculated intensities for the β^- decay of ^{50}Sc . Both experimental peaks are reproduced by the calculation although they are slightly shifted. Since the ^{50}Ca decay feeds an unique state and ^{50}Sc decays to just two, it is possible to use the experimental energies of the states to calculate the half-lives and to gauge the effect of the phase space. Proceeding in such a way, the new calculated half-lives for ^{50}Ca and ^{50}Sc are, respectively, $T_{\frac{1}{2}} = 12.3^{+0.3}_{-0.3} \text{ s}$ and $T_{\frac{1}{2}} = 120^{+2}_{-1} \text{ s}$ which improve the agreement with the experimental half-lives. These results are also shown in table 14.

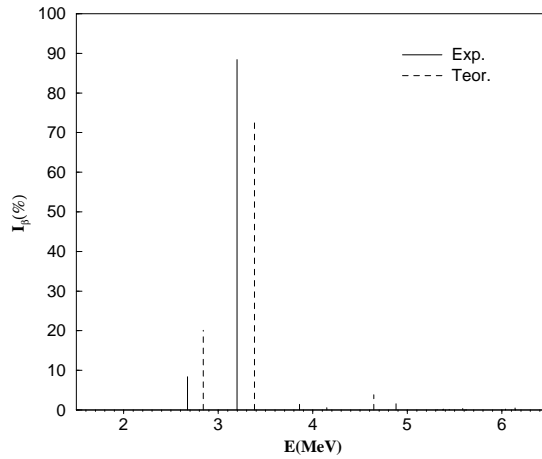


Fig. 24. Percentages of the β^- decay of ^{50}Sc . Experimental data from [32].

6.2 β^- decays in the isobar chain $A = 51$

Table 15 gathers the experimental and calculated half-lives for the isobar chain $A = 51$. The calculated values are quite close to the experimental ones.

Table 15

Half-lives of $A = 51$ isobars. Q_{β^-} values from [32].

A	J^π	$T_{1/2}$			$Q_{\beta^-}^{exp}(MeV)$
		KB3	KB3G	Exp.	
^{51}Ca	$\frac{3}{2}^-$	$8.9_{-0.9}^{+1.0} s$	$7.6_{-0.7}^{+0.8} s$	$10.0(8) s$	7.332(93)
^{51}Sc	$\frac{7}{2}^-$	$14.1_{-0.3}^{+0.3} s$	$10.4_{-0.2}^{+0.2} s$	$12.4(1) s$	6.508(20)
			$12.3 \pm 0.3 s$		
^{51}Ti	$\frac{3}{2}^-$	$6.94_{-0.02}^{+0.02} min$	$8.04_{-0.02}^{+0.02} min$	$5.76(1) min$	2.4706(15)
			$6.97 \pm 0.02 min$		
^{51}V			Stable		

Although within the Q_{β^-} energy window there is a large amount of Gamow-Teller strength (see figures 25, 26 and 27), the situation looks like in the $A = 50$ chain and much strenght is located around the Q_{β^-} values.

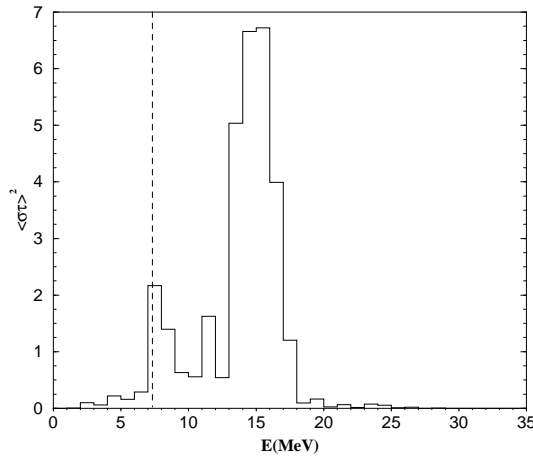


Fig. 25. Gamow-Teller strength after 50 iterations for the ^{51}Ca β^- decay. The $\langle \sigma\tau \rangle^2$ values are summed up in 1 MeV bins. The dashed line indicates the experimental Q_{β^-} value.

In figures 28 and 29 we compare the experimental percentages for the decays

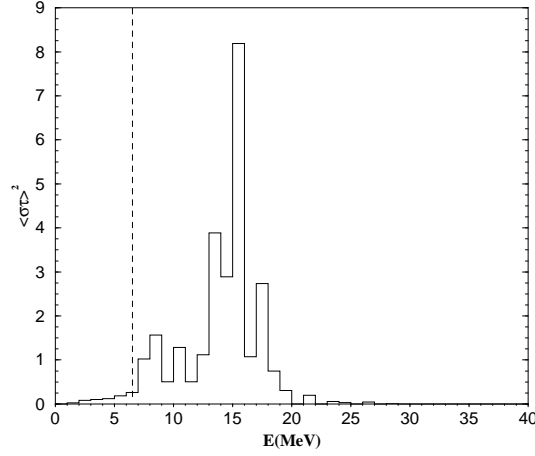


Fig. 26. Gamow-Teller strength after 50 iterations for the ^{51}Sc β^- decay. The $\langle \sigma \tau \rangle^2$ values are summed up in 1 MeV bins. The dashed line indicates the experimental Q_{β^-} value.

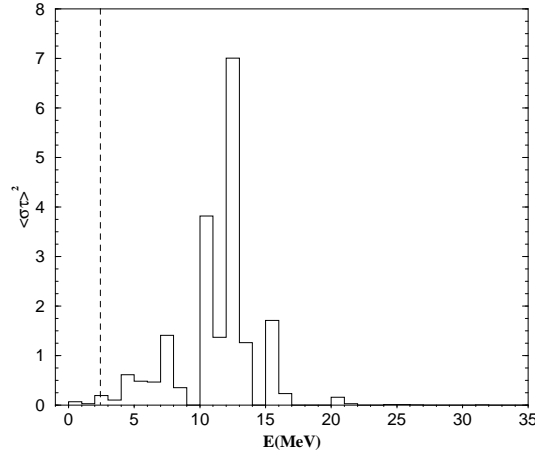


Fig. 27. Gamow-Teller strength after 50 iterations for the ^{51}Ti β^- decay. The $\langle \sigma \tau \rangle^2$ values are summed up in 1 MeV bins. The dashed line indicates the experimental Q_{β^-} value.

with the calculation for both ^{51}Ca and ^{51}Sc . In the latter, the agreement is very good. ^{51}Ca demands some comments. To compare with the experimental data we must keep in mind that only states up to 3.8 MeV in ^{51}Sc have been observed. In the first MeV there is a single experimental state fed by the decay. This fact is well reproduced by the calculation. Up to 3.5 MeV there are seven states experimentally observed in the decay, the same number is given by the calculation. However, the distribution of the intensity is not the same. In the calculation all the intensity is concentrated between 2.5 MeV and 3.0 MeV, while experimentally there are two states strongly fed at lower energy.

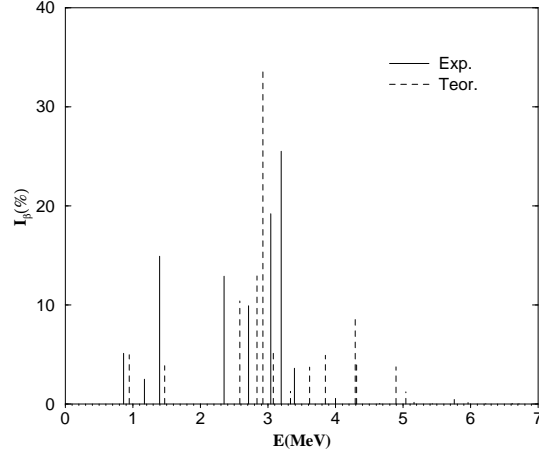


Fig. 28. Percentages of the β^- decay of ^{51}Ca . Experimental data from [32].

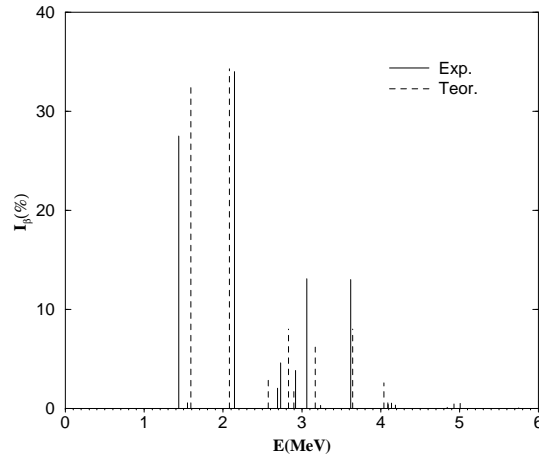


Fig. 29. Percentages of the β^- decay of ^{51}Sc . Experimental data from [32].

In the case of ^{51}Ti the decay only feeds two states in the daughter nucleus, a $J = \frac{3}{2}^-$ at 0.928 MeV (8.1(4)%) and a $J = \frac{5}{2}^-$ at 0.320 MeV (91.9(4)%). The calculation agrees with it since it predicts the decay to a $J = \frac{3}{2}^-$ state at 1.155 MeV (6.5%) and to another $J = \frac{5}{2}^-$ state at 0.457 MeV (93.5%).

In view of the comparison of the intensities for the decays of ^{51}Ca , ^{51}Sc and ^{51}Ti , it seems plausible to make a new analysis in the same terms we did in the previous section, i.e. to take the experimental energies for the four states strongly fed in ^{51}Sc and the corresponding two in ^{51}Ti . The new half-lives we obtain are $T_{\frac{1}{2}} = 12.3_{-0.3}^{+0.3} \text{ s}$ for ^{51}Sc and $T_{\frac{1}{2}} = 6.97_{-0.02}^{+0.02} \text{ min}$ for ^{51}Ti , in much better agreement with the experimental values shown in table 15. For ^{51}Ca this analysis is not so easy since the number of states fed is larger and it is

not simple to make a one to one correspondence between experimental and theoretical states.

6.3 β^- decays in the isobar chain $A = 52$

In table 16 the experimental data and the calculated results for the half-lives of the nuclei in the $A = 52$ isobar chain are shown. For ^{52}V we have only made a $t = 4$ calculation, because, to be consistent, the calculation in the daughter has to be $t = 5$. Going beyond that would have demanded an enormous computational effort. The theoretical half-lives compare reasonably well with the experimental numbers, although the discrepancy in ^{52}Ca is severe. We shall now analyse the intensity distributions and try to recompute the half-lives using as much as possible the experimental excitation energies.

Table 16

Half-lives of $A = 52$ isobars. Q_{β^-} values from [32].

A	J^π	$T_{\frac{1}{2}}$			$Q_{\beta^-}^{exp}(MeV)$
		KB3	KB3G	Exp.	
^{52}Ca	0^+	$0.8_{-0.3}^{+0.4} s$	$0.9_{-0.3}^{+0.5} s$	$4.6(3) s$	7.900(500)
			$1.38_{-0.4}^{+0.7} s$		
^{52}Sc	3^+	$8_{-1}^{+2} s$	$6.2_{-0.8}^{+1.0} s$	$8.2(2) s$	9.010(160)
^{52}Ti	0^+	$2.69 \pm 0.04 min$	$3.38 \pm 0.07 min$	$1.7(1) min$	1.973(8)
			$2.30 \pm 0.04 min$		
^{52}V	3^+	$5.544_{-0.014}^{+0.013} min$	$5.79 \pm 0.01 min$	$3.743(5) min$	3.9756(12)
			$4.87 \pm 0.01 min$		

Figure 30 shows the percentages for the ^{52}Ca β^- decay and figure 31 the same for ^{52}Sc . The ^{52}Ca case demands a special attention. When we analyzed the ^{52}Sc spectrum in section 5.2 we mentioned that there was one state without any experimental spin assignment at 675 keV (fig. 15). In [50] the calculation was made with the FPD6 interaction, producing a first $J = 1^+$ at 701 keV. It was suggested that it could correspond to the 675 keV state. Our interpretation of this state as the 2^+ member of the ground state multiplet is experimentally supported by the fact that if this state were a $J = 1^+$, it would have been observed in the β^- decay of ^{52}Ca . This is not the case, as can be seen in figure 30. On the contrary, most of the decay (86.8%) goes to the first experimental state with $J = 1^+$ assignment, corresponding to the one we obtain in the calculation. Thus, it is discarded that this unassigned experimental state

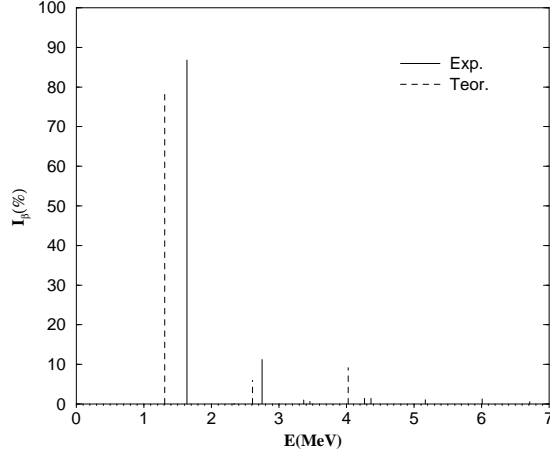


Fig. 30. Percentages of the β^- decay of ^{52}Ca . Experimental data from [32].

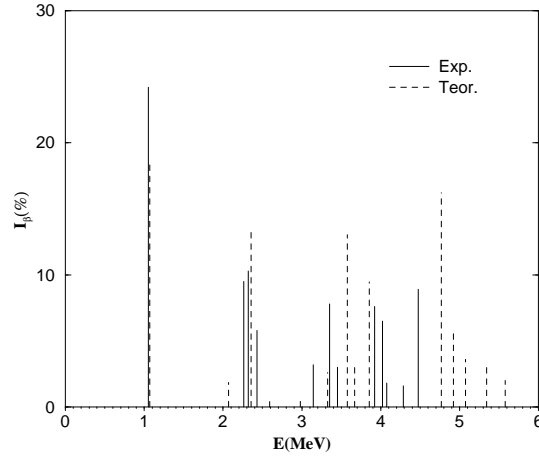


Fig. 31. Percentages of the β^- decay of ^{52}Sc . Experimental data from [32].

could be a $J = 1^+$. The first $J = 1^+$ corresponds to a configuration with a neutron in the $f_{5/2}$ orbit. As we said in the introduction, FPD6 locates the $1f_{5/2}$ orbit too low, producing a very low $J = 1^+$ state. The other three experimental $J = 1^+$ states are also fed through the decay of ^{52}Ca although with smaller intensity. The percentage of the second at 2.7 MeV is 11.2% while for the third at 3.5 MeV it is 0.6% and 1.4% for the last one at 4.3 MeV. These data help us to make a one to one correspondence between the states above 2 MeV in figure 15. Our third state $J = 1^+$ at 2.6 MeV corresponds to the second experimental one, our fourth $J = 1^+$ at 3.4 MeV to the third and the fourth experimental $J = 1^+$ to our sixth at 4.4 MeV.

The situation for ^{52}Sc in figure 31 is very satisfactory. The decay to the $J = 2^+$ excited state at 1 MeV and to the triplet around 2.3 MeV is well reproduced,

although in the calculation the triplet is more expanded than the experimental one. There is one state at 3.1 MeV without assigned spin, that seems to correspond to the 3^+ state near 3 MeV (the calculation predicts a 0.7% branch to it). The next branch goes to the second 4^+ at 3.3 MeV. Beyond, it becomes difficult to establish a detailed correspondence.

The decay of ^{52}Ti feeds (100%) a single state in the daughter nucleus ^{52}V , the $J = 1^+$ at 141 keV. This fact is reproduced properly by the calculation which predicts a 100% feeding of the $J = 1^+$ state at 300 keV in the daughter nucleus for the β^- decay of ^{52}Ti . On the other hand, ^{52}V decays 99.22(5)% to the $J = 2^+$ excited state of ^{52}Cr located at 1.4 MeV, what agrees with the calculation (a 98.92% feeds the $J = 2^+$ state at 1.5 MeV).

Finally, we recalculate the half-lives using the experimental energies of the single state fed in the decay of ^{52}Ti and ^{52}V , and of the two states fed in the decay of ^{52}Ca . For ^{52}Sc the analysis in these terms is not so easy. The new calculated half-lives are $T_{1/2} = 2.30 \pm 0.04 \text{ min}$ for ^{52}Ti and $T_{1/2} = 4.87 \pm 0.01 \text{ min}$ for ^{52}V . Both results improve the previous ones shown in table 16. For ^{52}Ca we get a half-life $T_{1/2} = 1.38^{+0.7}_{-0.4} \text{ s}$, reducing substantially the initial discrepancy.

7 Coulomb energy differences (CED) in the mirror pair ^{51}Mn - ^{51}Fe

It is well known that if the nucleon-nucleon interaction were charge symmetric the mirror nuclei would have the same level scheme. Thus, the small differences (normally a few tens of keV) in their excitation energies, are due to the isospin symmetry breaking Coulomb interaction. The analysis of this effect has been recently pushed up in mass, with the study of the $A=47$ and $A=49$ mirror pairs [53,54]. It was found that the CED's are extremely sensitive to the structure of the nuclear wave functions. The next step has been to measure the ^{51}Mn - ^{51}Fe mirror pair, the heaviest one in which high spin states up to the band termination have been observed [48].

In figure 32 the calculated spectra for both nuclei, including the Coulomb interaction are compared with the experimental data. The Coulomb matrix elements are those denoted "A42" in ref [54]. At this scale, very slight differences (hardly any) are appreciable between them. However, looking more carefully at the CED's an abrupt change is observed at $J = \frac{17}{2}^-$ (fig. 33). The effect is also present in the calculation, that shows exactly the same trends as the experiment, although with enhanced values. The large increase in the CED can be interpreted as due to the alignment of one proton pair in ^{51}Fe which does not occur in ^{51}Mn . As a consequence, the Coulomb energy is sharply reduced in ^{51}Fe but not in ^{51}Mn , therefore the CDE increases dramatically (in absolute value). The breaking of a proton pair occurs in ^{51}Fe because it has

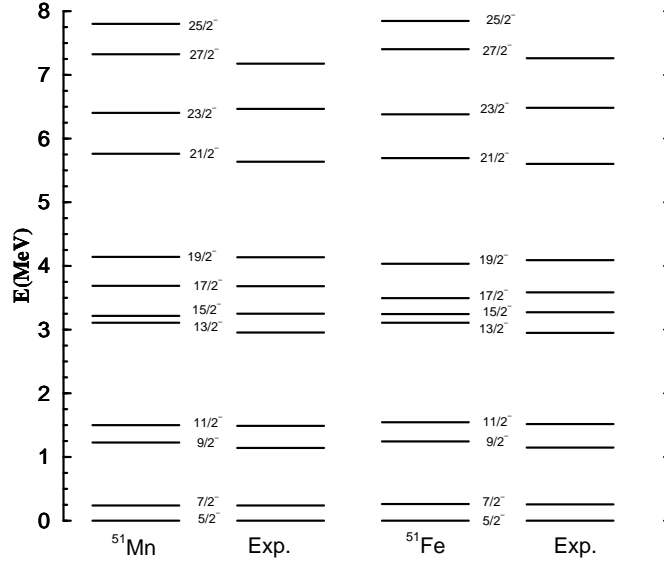


Fig. 32. Excitation energies of yrast bands of the mirror pair ^{51}Mn - ^{51}Fe . KB3G in the full pf -shell. Coulomb included.

an even number of protons while the odd proton in ^{51}Mn blocks the breaking process. In ^{51}Mn , a neutron pair is broken, but this has no effect in the Coulomb energy. Beyond $J = \frac{17}{2}^-$, the protons start aligning also in ^{51}Mn and therefore the CED's approach zero at the band termination.

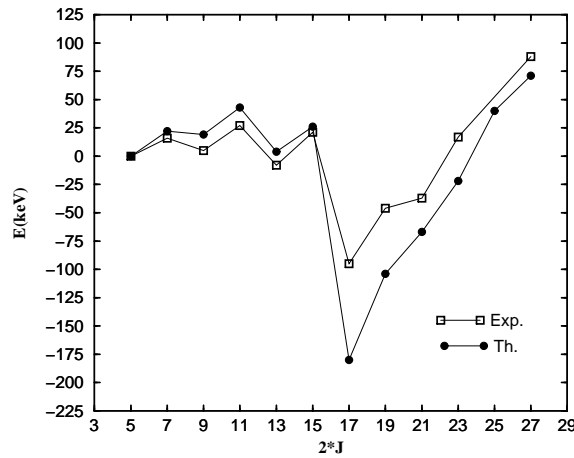


Fig. 33. Experimental and calculated CED defined as $E_x(^{51}\text{Fe}) - E_x(^{51}\text{Mn})$.

In order to make more visible the proton pair breaking, we have calculated the expectation value of the operator $H_{alin} = \left[(a_{\frac{7}{2}}^+ a_{\frac{7}{2}}^+)^{6,1}_{\pi\pi} (a_{\frac{7}{2}} a_{\frac{7}{2}})^{6,1}_{\pi\pi} \right]^0$ for the states of each nucleus. This operator acts as a sort of counter for the pairs of

$1f_{7/2}$ protons coupled to the maximum spin value $J = 6$. In figure 34 we have plotted the difference between its expectation values for the states of ^{51}Mn and ^{51}Fe . It is manifest that a proton pair fully aligns at $J = \frac{17}{2}^-$ in ^{51}Fe and not at all in ^{51}Mn .

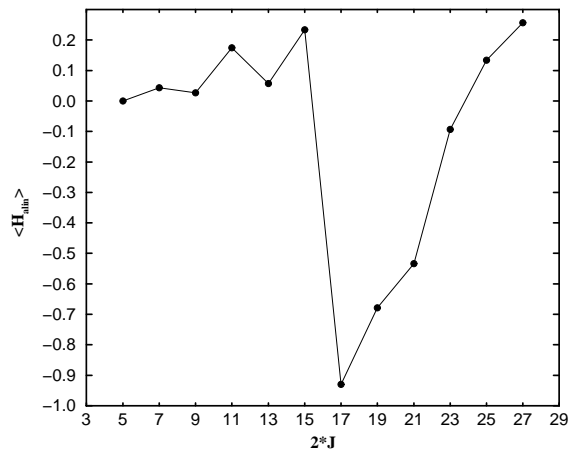


Fig. 34. Contribution from $1f_{7/2}$ proton pairs coupled to the maximum spin $J = 6$ (see text). ^{51}Mn minus ^{51}Fe .

The sudden change of structure at $J = \frac{17}{2}^-$ should also show up in the electromagnetic transitions. Indeed, this is the case and the general trend of the transition values up to $J = \frac{15}{2}^-$ breaks at $J = \frac{17}{2}^-$ dropping to nearly zero. For the $E2$ transitions we have $B(E2, \frac{17}{2}^- \rightarrow \frac{15}{2}^-) = 0.013 e^2 fm^4$, $B(E2, \frac{17}{2}^- \rightarrow \frac{13}{2}^-) = 2.012 e^2 fm^4$ and for the $M1$ transition $B(M1, \frac{17}{2}^- \rightarrow \frac{15}{2}^-) = 0.00002 \mu_N^2$, a reduction of several orders of magnitude that makes the state $\frac{17}{2}^-$ isomeric.

8 Magnetic moments of the N=28 isotones

New measures of the magnetic moments of the N=28 isotones [43,55] have brought up again the question of the sensitivity of these observables to the effective interactions and to the valence space truncations as well as the relevance of the use of bare or effective g -factors. We have examined this issue using the new interaction KB3G and we compare its results with those obtained using FPD6.

The ground and low-lying states of the N=28 isotones are dominated by $1f_{7/2}^n$ configurations. In the even-even cases, what is measured is the magnetic moment of the first excited 2^+ , therefore the closed shell nuclei ^{48}Ca and ^{56}Ni are

excluded from this systematics. In the $1f_{7/2}^n$ limit, the value of the 2^+ magnetic moment, which is the same for ^{50}Ti , ^{52}Cr and ^{54}Fe , is $3.31 \mu_N$, using bare g -factors. The usual choice of effective g -factors, $g_{eff}^s=0.75 g_{bare}^s$, $g_{\pi}^l=1.1 \mu_N$ and $g_{\nu}^l=-0.1 \mu_N$, gives $3.08 \mu_N$. For the odd isotones, the ground states have $J=7/2$ and $\mu=5.79 \mu_N$ with bare g -factors and $\mu=5.39 \mu_N$ with the effective g -factors. The differences amount to 7%. When mixing is allowed, the tendency is to reduce the difference between the results using bare and effective g -factors.

In table 17 we have collected the results for the even nuclei calculated with KB3G and FPD6 at different truncation levels. For KB3G, a large reduction (20%) occurs between $t=0$ and $t=3$, while a marginal 5% more is obtained in the full calculation. For FPD6 the reductions are larger (30% and 10% respectively). The FPD6 results are too small compared with the experiment even if bare g -factors are used, while those of KB3G are reasonably close to the measured values. The reason for the too large reduction that FPD6 produces can be related to the larger mixing with the $1f_{5/2}$ orbit, due to its very low location that we have already discussed. The experimental values of μ show a slight tendency to decrease with the number of protons, a trend that is weaker or even absent in the theoretical predictions.

Table 17

Magnetic moments of the first excited 2^+ states of the even $N=28$ isotones (in μ_N).

	^{50}Ti	^{52}Cr	^{54}Fe
EXP	2.89(15)	2.41(13)	2.10(12)
KB3G(full)(bare)	2.52	2.50	
KB3G($t=3$)(bare)	2.65	2.67	2.56
KB3G($t=3$)(eff)	2.49	2.57	2.52
FPD6(full)(bare)	2.28	1.90	
FPD6(full)(eff)	2.12	1.87	
FPD6($t=5$)(bare)	2.30	2.08	2.10
FPD6($t=5$)(eff)	2.14	2.04	2.12
FPD6($t=3$)(bare)	2.49	2.38	2.26
FPD6($t=3$)(eff)	2.32	2.32	2.29

In table 18 we present the results for the odd isotones. In this case KB3G seems to reproduce the decreasing trend better than FPD6, that gives a flatter behaviour. Considering the expected reductions in going from $t=3$ to the full calculation, the agreement can be considered quite decent, although in this case the use of effective g -factors worsens it. As in the case of the even isotones, FPD6 gives too small values.

Table 18

Magnetic moments of the $7/2^-$ ground states of the odd N=28 isobars (in μ_N).

	^{49}Sc	^{51}V	^{53}Mn	^{55}Co
EXP	–	5.15	5.02(1)	4.822(3)
KB3G(full)(bare)	5.34	4.99		
KB3G(t=3)(bare)	5.30	5.05	4.91	4.75
KB3G(t=3)(eff)	5.00	4.80	4.71	4.61
FPD6(t=3)(bare)	5.09	4.89	4.88	4.81
FPD6(t=3)(eff)	4.77	4.65	4.67	4.63

9 Conclusions

In this work we have extended our previous full pf -shell studies of the A=48 and A=49 isobars three units of mass. In order to be able to treat properly the N=Z=28 shell closure and its surroundings we have introduced a mass dependence in the interaction KB3 and refined its original monopole changes. This results in the KB3G interaction. G emphasizes that the new interaction produces the right quasiparticle gaps for all the N=28 isotones. With this interaction –that can be interpreted as a natural extension of KB3, equivalent to it for the nuclei studied already– we achieve an extremely high quality description of the abundant experimental data available in the mass region A=50/51/52. Besides, we are now in a much better situation concerning our predictive power for higher masses. We have also studied the beta decay of the isotopes of Ca, Sc, V and Ti, computing half-lives and strength distributions, that agree nicely with the experimental information too. In the final sections we dwell on the magnetic moments of the N=28 isotones and on the Coulomb displacement energies along the yrast band of the A=51 mirror nuclei.

Acknowledgements

This work has been partly supported by a grant of the DGES (Spain), ref. PB96-053 and by the IN2P3 (France)-CICyT (Spain) agreements. We also thank the CCCFC-UAM for a computational grant.

References

- [1] E. Caurier, A.P. Zuker, A. Poves, and G. Martínez-Pinedo, *Phys. Rev. C* **50** (1994) 225.
- [2] E. Caurier, J.L. Egido, G. Martínez-Pinedo, A. Poves, J. Retamosa, L.M. Robledo and A.P. Zuker, *Phys. Rev. Lett.* **75** (1995) 2466.
- [3] G. Martínez-Pinedo, A.P. Zuker, A. Poves and E. Caurier, *Phys. Rev. C* **55** (1997) 187.
- [4] S.M. Lenzi, C.A. Ur, D.R. Napoli, M.A. Nagarajan, D. Bazzacco, D.M. Brink, M.A. Cardona, G. de Angelis, M. De Poli, A. Gadea, D. Hojman, S. Lunardi, N.H. Medina and C. Rossi Alvarez, *Phys. Rev. C* **56** (1997) 1313.
- [5] C.A. Ur, D. Bucurescu, S.M. Lenzi, G. Martínez-Pinedo, D.R. Napoli, D. Bazzacco, F. Brandolini, D.M. Brink, J.A. Cameron, G. de Angelis, M. De Poli, A. Gadea, S. Lunardi, N. Mărgineau, M.A. Nagarajan, P. Pavan, C. Rossi Alvarez and C.E. Svensson, *Phys. Rev. C* **58** (1998) 3163.
- [6] F. Brandolini, N.H. Medina, S.M. Lenzi, D.R. Napoli, A. Poves, R.V. Ribas, J. Sánchez Solano, C.A. Ur, D. Bucurescu, M. De Poli, R. Menegazzo, D. Bazzacco, G. de Angelis, A. Gadea and C. Rossi Alvarez, *Phys. Rev. C* **60** (1999) 041305R.
- [7] A. Poves and J. Sánchez Solano, *Phys. Rev. C* **58** (1998) 179.
- [8] A. Poves and G. Martínez-Pinedo, *Phys. Lett. B* **430** (1998) 203.
- [9] D. Rudolph, C. Baktash, M.J. Brinkman, E. Caurier, D.J. Dean, M. Devlin, J. Dobaczewski, P.H. Heenen, H.Q. Jin, D.R. LaFosse, W. Nazarewicz, F. Nowacki, A. Poves, L.L. Riedinger, D.G. Sarantites, W. Satula and C.H. Yu, *Phys. Rev. Lett.* **82** (1999) 3763.
- [10] S.E. Koonin, D.J. Dean and K. Langanke, *Phys. Rep.* **278** (1997) 2.
- [11] S.E. Koonin, D.J. Dean and K. Langanke, *Ann. Rev. Nucl. Part. Sci.* **47** (1997) 463.
- [12] M. Honma, T. Mizusaki and T. Otsuka, *Phys. Rev. Lett.* **77** (1996) 3315.
- [13] T. Otsuka, M. Honma and T. Mizusaki, *Phys. Rev. Lett.* **81** (1998) 1588.
- [14] K. Hara, Y. Sun and T. Mizusaki, *Phys. Rev. Lett.* **83** (1999) 1922.
- [15] J. Terasaki, R. Wyss and P.H. Heenen, *Phys. Lett. B* **437** (1998) 1.
- [16] G. Martínez-Pinedo, A. Poves, L.M. Robledo, E. Caurier, F. Nowacki, J. Retamosa and A.P. Zuker, *Phys. Rev. C* **59** (1996) R2150.
- [17] C.E. Svensson, S.M. Lenzi, D.R. Napoli, A. Poves, C.A. Ur, D. Bazzacco, F. Brandolini, J.A. Cameron, G. de Angelis, M. De Poli, A. Gadea, D.S. Haslip, S. Lunardi, E.E. Maqueda, G. Martínez-Pinedo, N.A. Nagarajan, C. Rossi Alvarez and J.C. Waddington, *Phys. Rev. C* **58** (1998) R2621.
- [18] T.T.S. Kuo and G.E. Brown, *Nucl. Phys. A* **114** (1968) 235.

- [19] A. Poves and A. P. Zuker, Phys. Rep. **70** (1981) 235.
- [20] P. von Neumann-Cosel, A. Poves, J. Retamosa and A. Richter, Phys. Lett. B **443** (1998) 1.
- [21] A. R. Edmonds, *Angular Momentum in Quantum Mechanics* (Princeton University Press, Princeton, 1960).
- [22] I. S. Towner and J. C. Hardy, in *The Nucleus as a Laboratory for Studying Symmetries and Fundamental Interactions*, E. M. Henley and W. C. Haxton eds. (World-Scientific, Singapore, 1995); nucl-th/9504015.
- [23] D. H. Wilkinson and B. E. F. Macefield, Nucl. Phys. A **232** (1974) 58.
- [24] W. Bambynek, H. Behrens, M. H. Chen, B. Graseman, M. L. Fitzpatrick, K. W. D. Ledingham, H. Genz, M. Mutterer and R. L. Intemann, Rev. Mod. Phys. **49** (1977) 77.
- [25] E. Caurier, computer code ANTOINE, CRN, Strasburg, 1989.
- [26] E. Caurier and F. Nowacki, Acta Physica Polonica B, Vol. 30, 3 (1999) 705.
- [27] E. Caurier, G. Martínez-Pinedo, F. Nowacki, A. Poves, J. Retamosa and A. P. Zuker, Phys. Rev. C **59** (1999) 2033.
- [28] R. R. Whitehead, in *Moment methods in many fermion systems*, B. J. Dalton et al. eds. (Plenum, New York, 1980).
- [29] E. Caurier, A. Poves and A. P. Zuker, Phys. Lett. **256B** (1991) 301.
- [30] E. Caurier, A. Poves and A. P. Zuker, Phys. Lett. **252B** (1990) 13.
- [31] S. D. Bloom and G. M. Fuller, Nucl. Phys. A **440** (1985) 511.
- [32] Electronic version of Nuclear Data Sheets,
telnet://bnlnd2.dne.bnl.gov (130.199.112.132),
<http://www.dne.bnl.gov/nndc.html>.
- [33] M. Dufour and A. P. Zuker, Phys. Rev. C **54** (1996) 1641.
- [34] A. P. Zuker, J. Retamosa, A. Poves and E. Caurier, Phys. Rev. C **52** (1995) R1741.
- [35] A. Petrovici, K. W. Schmid and A. Faessler, Nucl. Phys. A **605** (1996) 290.
- [36] J. Duflo and A. P. Zuker, Phys. Rev. C **59** (1999) R2347.
- [37] W. A. Richter, M. J. Van Der Merwe, R. E. Julies and B. A. Brown, Nucl. Phys. A **523** (1991) 325.
- [38] A. P. Zuker and M. Dufour, archive LANL, nucl-th/9505012.
- [39] E. Caurier, G. Martínez-Pinedo, A. Poves and A. P. Zuker, Phys. Rev. C **52** (1995) R1736.
- [40] J. F. Berger, M. Girod and D. Gogny, Nucl. Phys. A **428** (1984) 23c.

- [41] T. González Llarena, *Ph.D. Thesis*, UAM Madrid, 1999.
- [42] R. B. Firestone, *Table of Isotopes* Vol. I and II, edited by V. S. Shirley (Wiley-Interscience, New York, 1996).
- [43] K.-H. Speidel, R. Ernst, O. Kenn, J. Gerber, P. Maier-Komor, N. Benczer-Koller, G. Kumbartzki, L. Zamick, M. S. Fayache, and Y. Y. Sharon, *Phys. Rev. C* **62** (2000) 031301R.
- [44] A. Novoselsky, M. Vallières and O. La'adan, *Phys. Rev. Lett.* **79** (1997) 4341.
- [45] Y. Utsuno, T. Sebe, T. Otsuka and T. Mizusaki, *Phys. Rev. Lett.* **81** (1998) 5948.
- [46] A. Novoselsky, M. Vallières and O. La'adan, *Phys. Rev. Lett.* **81** (1998) 5949.
- [47] A. Novoselsky, M. Vallières and O. La'adan, *Phys. Rev. Lett.* **81** (1998) 5955.
- [48] M. A. Bentley, S. J. Williams, D. T. Joss, C. D. O'Leary, A. M. Bruce, J. A. Cameron, P. Fallon, L. Frankland, W. Gelletly, C. J. Lister, G. Martínez-Pinedo, A. Poves, P. H. Regan, P. Reiter, B. Rubio, J. Sánchez Solano, D. Seweryniak, C. E. Svensson, S. M. Vicent and D. D. Warner, *Phys. Rev. C*, **62** (2000) 051303R.
- [49] A. Huck, G. Klotz, A. Knipper, C. Miehe, C. Richard-Serre, G. Walter, A. Poves, H. L. Ravn and G. Marguier, *Phys. Rev. C* **31** (1985) 2226.
- [50] A. Novoselsky and M. Vallières, *Phys. Rev. C* **57** (1998) R19.
- [51] D. E. Appelbe, J. Sánchez Solano, J. A. Cameron, J. Chenkin, T. E. Drake, B. Djerroud, S. Filibotte, A. Poves, J. C. Waddington and D. Ward, to be published.
- [52] M. Axiotis *et al.*, to be published.
- [53] C. D. O'Leary, M. A. Bentley, D. E. Appelbe, D. M. Cullen, S. Ertürk, R. A. Bark, A. Maj and T. Saitoh, *Phys. Rev. Lett.* **79** (1997) 4349.
- [54] M. A. Bentley, C. D. O'Leary, A. Poves, G. Martínez-Pinedo, D. E. Appelbe, R. A. Bark, D. M. Cullen, S. Ertürk and A. Maj, *Phys. Lett. B* **437** (1998) 243; erratum in *Phys. Lett. B* **451** (1999) 445.
- [55] R. Ernst, K.-H. Speidel, O. Kenn, U. Nachum, J. Gerber, P. Maier-Komor, N. Benczer-Koller, G. Jakob, G. Kumbartzki, L. Zamick and F. Nowacki, *Phys. Rev. Lett.* **84** (2000) 416.